Journal of Medicinal Chemistry

Article

pubs.acs.org/jmc

2-Hexylthio-β,γ-CH_2-ATP is an Effective and Selective NTPDase2 Inhibitor

Irina Gillerman,[†,⊥] Joanna Lecka,[‡,§,⊥] Luba Simhaev,[†,⊥] Mercedes N. Munkonda,[‡,§] Michel Fausther,[‡,§] Mireia Martín-Satué,[‡,§,∥] Hanoch Senderowitz,*[,†] Jean Sévigny,*[,‡,§] and Bilha Fischer*[,†]

[†]Department of Chemistry, Bar-Ilan University, Ramat-Gan 52900, Israel

[‡]Département de microbiologie-infectiologie et d'immunologie, Faculté de Médecine, Université Laval, Québec City, Québec, Canada

[§]Centre de recherche du CHU de Québec, Québec City, Québec, Canada

[∥]Department of Pathology and Experimental Therapeutics, University of Barcelona, Barcelona, Spain

S *Supporting Information*

ABSTRACT: NTPDase2 catalyzes nucleoside triphosphates and consequently, through the interaction of nucleotides with P2 receptors, controls multiple biological responses. NTPDase2 inhibitors could modulate responses induced by nucleotides in thrombosis, inflammation, cancer, etc. Here we developed a set of ATP analogues as potential NTPDase inhibitors and identified a subtype-selective and potent NTPDase2 inhibitor, 2-hexylthio-β,γ-methylene-ATP, **2**. Analogue **2** was stable to hydrolysis by NTPDase1, -2, -3, and -8. It inhibited hNTPDase2 with K_i 20 μM, while only marginally (5−15%) inhibiting NTPDase1, -3, and -8. Homology models of hNTPDase1 and -2 were constructed. Docking and subsequent linear interaction energy (LIE) simulations provided a correlation with r^2 = 0.94 between calculated and experimental inhibition data for the triphosphate analogues considered in this work. The origin of selectivity of **2** for NTPDase2 over NTPDase1 is the thiohexyl moiety of **2** which is favorably located within a hydrophobic pocket, whereas in NTPDase1 it is exposed to the solvent.

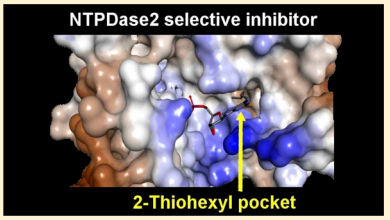

INTRODUCTION

Hydrolysis of extracellular nucleotides plays a critical role in physiological phenomena, by creating a balance between the excitatory actions of ATP (and ADP) at P2 receptors and the often inhibitory actions of its breakdown product, adenosine, at P1 receptors. NTPDases, EC 3.6.1.5,[1−3] are responsible for the rapid hydrolysis of the extracellular nucleotides.[3] Eight members of the E-NTPDase family are known (NTPDase1−8) among which four are membrane-bound glycoproteins with an extracellular active site (NTPDase1−3, −8).[52] NTPDase2 is expressed in several tissues. In the vasculature it is expressed in the adventitia of arteries and on subendothelial cells of veins where it was proposed to facilitate platelet aggregation.[6] Indeed, upon injury, large amounts of ATP are secreted to the extracellular milieu and are converted to the platelet activation factor, ADP, by NTPDase2, thus activating $P2Y_1$ and $P2Y_{12}$ receptors on thrombocytes.[6]

An imbalanced ATP/ADP hydrolysis ratio, in favor of ATP,[7] was observed in patients with coronary artery disease leading to prothrombotic ADP levels which could not be effectively removed. In addition, ADP (as well as ATP and ADP-α,β-CH_2) potently inhibits ecto-5′-nucleotidase,[4−7] thereby preventing the extracellular formation of adenosine and impeding adenosine receptor-effected vasodilation and antithrombotic properties.[8−10]

Specific localization of NTPDase2 in the heart suggests that this enzyme may regulate functions other than platelet activation. Extracellular ATP, and its degradation product, adenosine, exert pronounced inotropic and chronotropic actions and influence electrical impulse conduction as well as metabolic processes.[11,14] Thus, a selective inhibitor for NTPDase2 may exhibit cardioprotective properties.

In the central nervous system, NTPDase2 is expressed on astrocytes.[11] During cerebral ischemia, extracellular ATP concentrations rise and it is predominantly hydrolyzed by NTPDase2. The resulting ADP is a potent inhibitor of ecto-5′-nucleotidase. This enzyme dephosphorylates AMP to the cytoprotective adenosine.[12] Thus, NTPDase2 inhibitors may be useful for the treatment of ischemic conditions in brain.

There is an accumulating evidence of overexpression of NTPDase2 in gliomas.[13] Because ADP derived from NTPDase2 activity stimulates platelet migration to the tumor area, NTPDase2, by regulating angiogenesis and inflammation, seems to play an important role in tumor progression.

Taken together, selective and potent NTPDase2 inhibitors may serve as potential drug candidates for the treatment of health disorders such as thrombosis, ischemia, and cancer. Ideally, NTPDase inhibitors should have no effect on P2 receptors and should be stable to hydrolysis by ectonucleotidases. So far only a few NTPDase inhibitors have been described in the literature. Recently we reported on BuS-adenine nucleotide analogues that specifically inhibit NTPDase1[14,15] and are not agonists of P2Y receptors. Other non P2 receptor agonist reported inhibitors are ARL 67156,[16,17] polyoxometalates

Received: December 18, 2013
Published: June 27, 2014

(POMs),[15] and PSB-6426 (K_i 8.2 μM).[18] However, these compounds are not NTPDase-subtype selective.

Here, we report on the synthesis and evaluation of a series of adenosine 5′-tri- and -monophosphate analogues as potential and selective inhibitors of NTPDase2. Specifically, we studied the inhibitory effect of analogues **1**−**9** on NTPDase-1, -2, -3, -8 and evaluated their selectivity vs NPP1 and NPP3. Next, we determined the K_i value of the most promising and selective NTPDase2 inhibitor and studied its inhibition of ATPase activity on various cell surfaces. Finally, we studied computationally the most active and the least active compounds identified here together with NTPDase1 inhibitors previously reported by us, and tested for NTPDase2 inhibition,[17] to develop a model for predicting NTPDase2 inhibition by nucleotide analogues.

EXPERIMENTAL SECTION

General. All air- and moisture-sensitive reactions were carried out in flame-dried, argon-flushed, two-necked flasks sealed with rubber septa, and the reagents were introduced with a syringe. TLC analysis was performed on precoated Merck silica gel plates (60F-254). Visualization was accomplished with UV light. New compounds were characterized (and resonances assigned) with proton nuclear magnetic resonance using AC-200 spectrometers, Bruker DPX-300, or DMX-600. ^{1}H NMR spectra were recorded in D_2O, and the chemical shifts are reported in ppm relative to HDO (4.78 ppm) as an internal standard. Nucleotides were also characterized with ^{31}P NMR in D_2O, using 85% H_3PO_4 as an external reference, on a AC-200 spectrometer at pH 8. All final products were characterized on an AutoSpec-E Fision VG high-resolution mass spectrometer with chemical ionization and high-resolution mass spectrometry. Nucleotides were desorbed from a glycerol matrix under FAB (fast atom bombardment) conditions in low and high resolution. Primary purification of the nucleotides was achieved on an LC (Isco UA-6) system using a Sephadex DEAE-A 25 column, which was swelled in 1 M $NaHCO_3$ at RT overnight. Final purification of the nucleotides was achieved on a high-performance liquid chromatography (HPLC) (Merck-Hitachi) system with a semi-preparative reverse-phase (Gemini 5 μm C-18 110 Å 250 × 10 mm, Phenomenex, Torrance, CA). For analytical purposes, a Gemini (5 μm, C-18, 110 Å, 150 × 4.6 mm, Phenomenex, Torrance, CA) was used. The purity of the nucleotides was evaluated on an analytical column in two different solvent systems. Peaks were detected by UV absorption using a diode array detector. Solvent system I consisted of (A) CH_3CN and (B) 0.1 M TEAA (pH 7). Solvent system II consisted of (A) 5 mM tertabutylammonium phosphate (TBAP) in methanol and (B) 60 mM ammonium phosphate and 5 mM TBAP in 90% water/10% methanol. See gradient details below. 2-Hexylthioadenosine[22] and 8-azaadenosine[19] were prepared according to literature methods.

2-Hexylthioadenosine-5′-(β,γ-methylene-triphosphate), 2. 2-Hexylthioadenosine[20] (120 mg, 0.31 mmol) was dissolved in dry trimethyl phosphate (1 mL) and cooled to −15 °C. Proton sponge was added (105 mg, 0.49 mmol, 1.6 equiv). After the mixture was stirred for 20 min, $POCl_3$ (85 μL, 0.93 mmol, 3 equiv) was added dropwise, and the reaction mixture was stirred for 2 h. A solution of 1 M bis-tributylammionium salt of methylene diphosphonic acid in DMF (2.2 mL, 2.2 mmol, 7 equiv) and Bu_3N (300 μL, 1.26 mmol, 4 equiv) was added at once. After the mixture was stirred for 6 min, 1 M TEAB (5 mL) was added, and the clear solution was stirred for 45 min at RT. The solution was freeze-dried. The semisolid obtained after freeze-drying was chromotographed on an activated Sephadex DEAE-A 25 column using a two-step gradient of NH_4HCO_3 (200 mL of 0−0.2 M and then 350 mL of 0.2−0.4 M). The relevant fractions were freeze-dried repeatedly to yield the product as a white solid in a 70% yield. Final separation was achieved by HPLC, applying a linear gradient of TEAA/CH_3CN 80:20 to 60:40 in 25 min (flow rate 6 mL/min), retention time (t_R) 15.7 min (98% purity); linear gradient of phosphate buffer/CH_3CN 80:20 to 60:40 in 15 min (flow rate 1 mL/min), t_R 4.3 min (91% purity). ^{1}H NMR (D_2O, 600 MHz) δ: 8.35 (s, 1H, H2), 6.1 (d, 1H, J = 6.0 Hz,, H1′), 4.54 (t, 1H, J = 2.4 Hz, H2′), 4.36 (m, 1H, H3′), 4.2 (m, 1H, H4′), 3.1 (m, 2H, H5′, H5″), 3 (t, 2H, J = 15.0 Hz, SCH_2), 2.3 (t, 2H, J = 20.4 Hz CH_2 phosphonate), 1.73 (m, 2H, SCH_2CH_2), 1.45 (m, 2H, $SCH_2CH_2CH_2$), 1.2 (m, 2H, $SCH_2CH_2CH_2CH_2$), 0.96 (m, 2H, $SCH_2CH_2CH_2CH_2CH_2$), 0.90 (3H, CH_3) ppm; ^{31}P NMR (D_2O, 121 MHz, pH 8.5) δ: 15 (s), 9.8 (m), −10.2 (d) ppm; MS (TOF ES$^-$): 617 (M^-H^+); HRMS: calcd for $C_{17}H_{26}N_5O_{12}P_3S$ 617.4031 found, 617.5034.

***N*$^{6′}$,*N*$^{6″}$-Diethyladenosine, 16.** 6-Chloropurine riboside 2′,3′,5′-triacetate (382 mg, 0.93 mmol) was dissolved in DMF (7 mL), and diethylamine was added (290 μL, 2.8 mmol, 3 equiv). The reaction mixture was stirred for 24 h at 60−70 °C in a sealed tube. The solvent was evaporated, and the residue was triturated with ethanol. The mixture was separated on a silica gel column eluted with chloroform. The product was obtained in a 27% yield (80 mg). ^{1}H NMR (CD_3OD, 300 MHz) δ: 8.20 (s, 1H, H8), 8.10 (s, 1H, H2), 6.00 (d, 1H, J = 5 Hz, H1′), 4.90 (br s, 4H) 4.75 (m, 1H, J = 5 Hz, H2′), 4.2 (m, 1H, H3′), 3.87 (m, 2H, H5′, H5″), 3.85 (m, 3H, H4′, NCH_2) 1.26 (t, J = 6.9 Hz, 6H) ppm; ^{13}C NMR (CD_3OD, 50.3 MHz) δ: 154.31 (C-6), 152.2 (C-2), 150.9 (C-4), 141.58 (C-2), 120.3 (C-5), 89.3 (C-1′), 86.4 (C-4′), 74.13 (C-2′), 72.6 (C-3′), 62.4 (C-5′) 43.40 ($2CH_2$), 13.01 ($2CH_3$) ppm; MS (TOF ES$^+$): 324 (M^-H^+). HRMS: calcd for $C_{14}H_{21}N_5O_4$ 323.1476 found, 323.1608.

***N*$^{6′}$,*N*$^{6″}$-Dibenzyladenosine, 17.** 6- Chloropurine riboside 2′,3′,5′-triacetate (296 mg, 0.64 mmol) was dissolved in DMF (7 mL), and dibenzylamine was added (371 μL, 1.93 mmol, 3 equiv). The reaction mixture was stirred for 24 h at 60−70 °C. The mixture was evaporated and separated on a silica column with 90:10 $CHCl_3$:MeOH. The product was obtained in a 44% yield (127 mg). Spectroscopic data were consistent with that from the literature.[21]

Phosphorylation Reaction. General Procedure. Nucleotides **1**, **6**, 7, and **11** were prepared by our previously published procedure.[22]

8-Aza-2-hexylthioadenosine 5′-triphosphate, ***1****,*. was obtained as an off-white solid at a 52% yield (100 mg, 0.16 mmol) from 8-aza-2-hexylthioadenosine (120 mg, 0.31 mmol) yield. Final separation was achieved on HPLC, applying a linear gradient of TEAA/CH_3CN 70:30 to 55:45 in 25 min (flow rate 6 mL/min), t_R 14 min (92% purity). Compound purity was evaluated by applying a linear gradient of 50 mM phosphate buffer (pH = 7)/CH_3CN 70:30 to 60:40 in 25 min (flow rate 1 mL/min) t_R 4.5 min (90% purity). ^{1}H NMR (D_2O, 300 MHz) δ: 6.15 (d, 1H, J = 4.5 Hz, H1′), 4.49 (t, 1H, J = 4.8 Hz, H2′), 4.43 (m, 1H, H3′), 4.3 (m, 1H, H4′), 3.12 (m, 2H, H5′, H5″), 3.03 (m, 2H, SCH_2), 1.73 (m, 2H, SCH_2CH_2), 1.45 (m, 2H, $SCH_2CH_2CH_2$), 1.2 (m, 2H, $SCH_2CH_2CH_2CH_2$), 0.96 (m, 2H, $SCH_2CH_2CH_2CH_2CH_2$), 0.9 (3H, CH_3) ppm; ^{31}P NMR (D_2O, 81 MHz, pH 8.5) δ: −23 (t), 10.2 (d), −9.8 (d) ppm; MS (TOF ES$^-$): 620 (M^+H^-). HRMS: calcd for $C_{15}H_{23}N_6O_{13}P_3S$, 620.3640; found, 620.3420.

N*$^{6′}$,*N*$^{6″}$-Diethyladenosine 5′-triphosphate,** ***6*,*. was obtained as a white solid at a 73% yield (81 mg, 0.15 mmol) starting from *N*$^{6′}$,*N*$^{6″}$-diethyladenosine, **21** (65 mg, 0.2 mmol). Final purification was achieved on HPLC, applying a linear gradient of TEAA/CH_3CN 88:12 to 78:22 in 25 min (flow rate 6 mL/min), t_R 14 min (99.8% purity); linear gradient of phosphate buffer/CH_3CN 95:5 to 90:10 t_R 4 min (92% purity). ^{1}H NMR (D_2O, 300 MHz) δ: 8.46 (s, 1H, H2), 8.2 (s, 1H, H8), 6.11 (d, 1H, J = 5.5 Hz, H1′), 4.8 (t, 1H, J = 5.5 Hz, H2′), 4.45 (m, 1H, H3′), 4.35 (m, 1H, H4′), 4.2 (m, 2H, H5′, H5″), 3.8 (m, 4H, CH_2), 1.4 (t, 6H, J = 6.7 Hz, CH_3) ppm; ^{31}P NMR (D_2O, 81 MHz, pH 8.5) δ: −10 (d), −10.5 (d), −22.5 (t) ppm; MS (TOF ES$^+$): 560 (M^+H^-). HRMS: calcd for $C_{14}H_{20}N_5O_{13}P_3$, 559.0304; found, 559.0271.

N*$^{6′}$,*N*$^{6″}$-Dibenzyladenosine 5′-triphosphate,** ***7*,*. was obtained as a white solid at a 68% yield (70 mg) starting from *N*$^{6′}$,*N*$^{6″}$-dibenzyladenosine (127 mg, 0.28 mmol). Final purification was achieved on HPLC, applying a linear gradient of TEAA/CH_3CN 70:30 to 55:45 in 25 min (6 mL/min), t_R 14 min (90% purity) linear gradient of phosphate buffer/CH_3CN 80:20 to 60:40 in 25 min (1 mL/min) t_R 5 min (92% purity). Spectral data were consistent with that from the literature.[23]

dx.doi.org/10.1021/jm401933c | J. Med. Chem. 2014, 57, 5919−5934

8-Azaadenosine 5′-triphosphate,[23] ***11,***. was prepared from 8-azaadenosine (25.7 mg, 0.096 mmol) and obtained at a 45% yield.[22] Spectral data were consistent with that from the literature.[25]

Plasmids. The plasmids used in this study have all been described in published reports: human NTPDase1 (GenBank accession no. U87967),[24] human NTPDase2 (NM_203468), human NTPDase3 (AF034840),[25] human NTPDase8 (AY430414),[26] human ecto-5′-nucleotidase (NM_002526),[27] human NPP1 (NM_006208),[28] and human NPP3 (NM_005021).[29]

Cell Transfection and Protein Preparation. COS-7 cells were transfected with an expression vector (pcDNA3) containing the cDNA encoding for each NTPDase using lipofectamine (Invritrogen) and harvested 40−72 h later, as previously described.[24] For the preparation of protein extracts, transfected cells were washed three times with Tris-saline buffer at 4 °C, collected by scraping in harvesting buffer (95 mM NaCl, 0.1 mM PMSF, and 45 mM Tris, pH 7.5) and washed twice by centrifugation (300*g*, 10 min, 4 °C). The cells were then resuspended in the harvesting buffer supplemented with 10 μg/mL aprotinin to block proteinases and sonicated. Nucleus and cellular debris were discarded by another centrifugation (300*g*, 10 min, 4 °C), and the resulting supernatant (thereafter called protein extract) was aliquoted and stored at −80 °C until used. Protein concentration in the protein extracts was estimated by Bradford microplate assay using bovine serum albumin as a standard.[30]

Enzymatic Activity Assays. *NTPDases (EC 3.6.1.5) and Ecto-5′-nucleotidase (EC 3.1.3.5).* Activity was measured as described previously[3] in 0.2 mL of incubation medium (5 mM $CaCl_2$ and 80 mM Tris, pH 7.4) or Tris-Ringer buffer (in mM, 120 NaCl, 5 KCl, 2.5 $CaCl_2$, 1.2 $MgSO_4$, 25 $NaHCO_3$, 5 mM glucose, 80 Tris, pH 7.4) at 37 °C with or without analogues **2**−**9**. Ectonucleotidase protein extracts were added to the incubation mixture and preincubated at 37 °C for 3 min. The reaction was initiated by the addition of 10−100 μM ATP or AMP for NTPDases and ecto-5′-nucleotidase, respectively, with or without analogues and stopped after 15 min with 50 μL of malachite green reagent. The released inorganic phosphate (P_i) was measured at 630 nm according to Baykov et al.[31] The type of inhibition was determined by Dixon[32] and Cornish−Bowden[35] plots of four independent experiments, and K_i values were obtained using nonlinear regression.

Protein extracts from nontransfected COS-7 cells exhibited ATP or AMP hydrolysis less than 5% of that of COS-7 cells transfected with either NTPDases or ecto-5′-nucleotidase expressing plasmid. Hence, NTPDase or ecto-5′-nucleotidase activity of native COS-7 cells was considered as negligible.

NPPs (EC 3.1.4.1; EC 3.6.1.9). Evaluation of the effect of **2** on human NPP1 and NPP3 activity was carried out with *p*-nitrophenylthymidine 5′-monophosphate (pNP-TMP) as the substrate.[28,33] The reactions were carried out at 37 °C in 0.2 mL of the following incubation mixture, in mM: 1 $CaCl_2$, 140 NaCl, 5 KCl, and 50 Tris, pH 8.5, with or without analogues. Analogues **2** and pNP-TMP were used at a concentration of 100 μM. Human NPP1 or NPP3 extract was added to the incubation mixture and preincubated at 37 °C for 3 min. Reaction was started by adding pNP-TMP, and the production of *p*-nitrophenol was measured at 410 nm, after 15 min. The protein extracts from nontransfected COS-7 cells exhibited less than 5% of pNP-TMP hydrolysis after transfection with either NPP1 or NPP3 expressing plasmid and, as such, their NPP1/3 activity was considered as negligible.

Statistical Analysis. Statistical analysis was performed with Student's *t* test (Microsoft Office OneNote 2003). *P* values below 0.05 were considered statistically significant.

Homology Modeling of NTPDase2. A ligand-supported model of human NTPDase2 was built based on the crystal structure of rat NTPDase2[34] (PDB code 3CJA; sequence identity to human NTPDase2 of 82%). This template was selected because of its favorable resolution (2.1 Å) and because it was solved in the presence of an ATP analogue (AMPPNP) and a cofactor (Ca^{2+}). The sequence of the target protein (accession number Q9Y5L3) was downloaded from the UniprotKB/Swiss-Prot[35] server and aligned with the target sequence using the ClustalW[36] method as implemented in Discovery

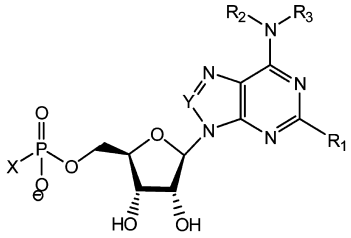

Compound	Y	R_1	R_2	R_3	X
1	N	HexS	H	H	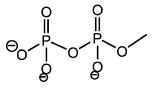
2	C	HexS	H	H	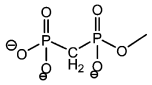
3	N	H	H	H	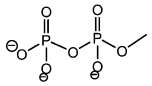
4	C	H	Me	H	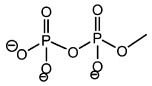
5	C	H	Me	Me	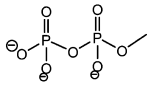
6	C	H	Et	Et	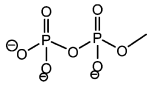
7	C	H	Bz	Bz	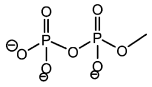
8	C	H	Me	Me	-O
9	C	H	Et	Et	-O

Figure 1. Adenosine mono- and triphosphate analogues **1**−**9** explored in this study.

Studio (DS) version 2.5.5[37] using default settings. Six conserved water molecules within the catalytic site of the NTPDase2 were identified by superposing four structures of *Rattus norvegicus* NTPDase2 (PDB codes: 3CJ1, 3CJA, 3CJ7, 3CJ9) based on multiple sequence alignment using DS protocols, and their coordinates were used in course of the homology modeling procedure. Two of these water molecules are involved in the catalytic reaction, while the additional four coordinate the Ca^{2+} ion in the catalytic site.[34] These water molecules are also largely conserved in the crystal structures of Legionella pneumophila and *Toxoplasma gondii* NTPDase1. The alignment, the conserved water molecules, and the crystal ligand were used as input to the MODELER[12] program as implemented in DS version 2.5.5. Default settings were used throughout the modeling procedure (optimization level = high; no. of models =10; refine loops = false). The highest ranked model was tested for stereochemical quality using Procheck[42] and Prosa,[38,39] and selected for subsequent analysis.

Homology Modeling of NTPDase1. A ligand-supported model of human NTPDase1 was built in a manner similar to that described above for NTPDase2 using the NTPDase1 sequence (accession number P49961) and the rat NTPDase2 structure (sequence identity to human NTPDase1 of 44%).

Docking. Docking simulations were performed using Glide[40−42] XP (extra precision sampling and scoring using the OPLS-AA force field with energy penalties for nonplanar amide bonds; flexible ligand

dx.doi.org/10.1021/jm401933c | J. Med. Chem. 2014, 57, 5919−5934

Scheme 1. Synthesis of 2-Hexylthio-β,γ-methylene-ATP Analogues 1 and 2[a]

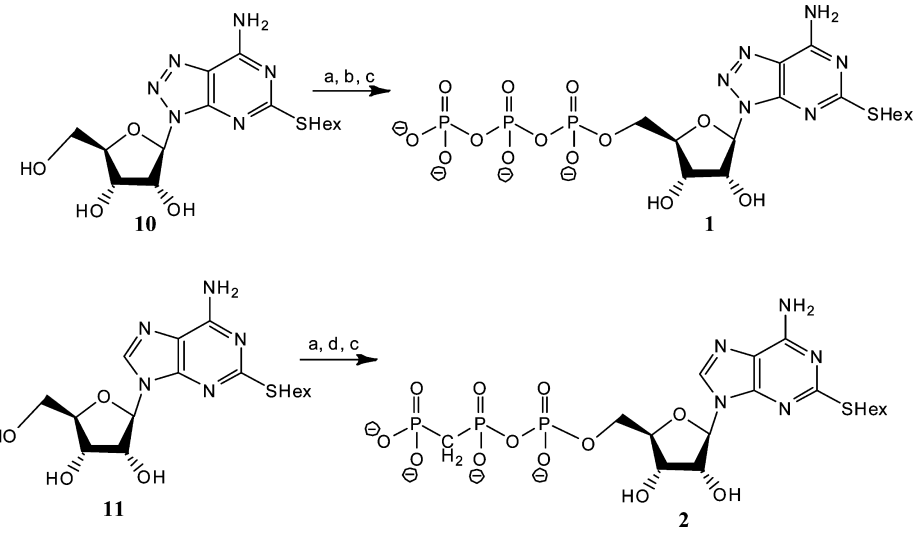

[a]Reagents and conditions: (a) $POCl_3$, proton sponge, −15 °C, 2 h; (b) $(NHBu_3)H_2P_2O_7/NBu_3$, −10 °C, 6 min; (c) 1 M TEAB, RT, 45 min, overall yield of 1:52%; (d) $(Bu_3NH)_2CH_2P_2O_6H_2/NBu_3$, −10 °C, 6 min, overall yield for **2**, 70%.

Scheme 2. Synthesis of N^6-Substituted ATP and AMP Analogues 4 and 9[a]

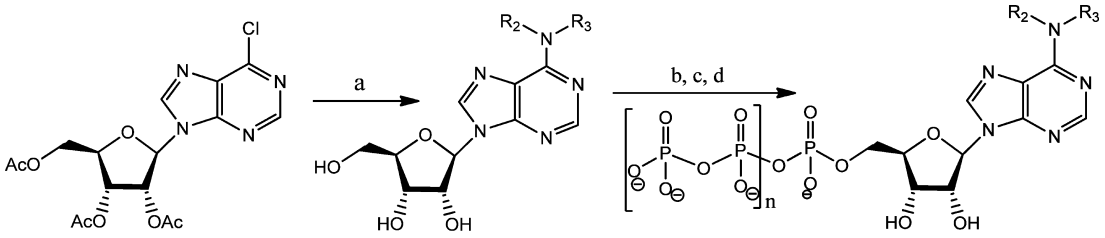

14 R_2 = Me R_3 = H
15 R_2 = Me R_3 = Me
16 R_2 = Et R_3 = Et
17 R_2 = Bz R_3 = Bz

4 n = 1 R_2 = Me R_3 = H
5 n = 1 R_2 = Me R_3 = Me
6 n = 1 R_2 = Et R_3 = Et
7 n = 1 R_2 = Bz R_3 = Bz
8 n = 0 R_2 = Me R_3 = Me
9 n = 0 R_2 = Bz R_3 = Bz

[a]Reagents and conditions: (a) NHR_2R_3/EtOH, 100 °C, 16 h (70% for **14**, 50% for **15**, 27% for **16**, 44% for **17**); (b) $POCl_3$, proton sponge, −15 °C, 2 h; (c) $(NHBu_3)H_2P_2O_7/NBu_3$, −10 °C, 6 min; (d) 1 M TEAB, RT, 45 min, overall yield for steps b−d: 74% for **4**, 73% for **5**, 73% for **6**, 68% for **7**, 30% for **8**, and 32% for **9**.

with sampling of nitrogen inversion and ring conformation, keeping the best 800 poses for postdocking minimization) as implemented in Maestro 9.0,[43] and were initiated from ligand-specific conformational ensembles generated with the LMCS/MCMM conformational search procedure as implemented in Maestro 9.0.[49] Prior to docking, the model was prepared using the protein preparation wizard in Maestro 9.0. Both lowest energy poses and poses with binding modes similar to the crystallographic ligand (AMPPNP) were selected for further analysis.

LIE Calculations. Linear interaction energy (LIE)[44,45] calculations were performed using the program Q[46] and the OPLS-AA 2001[47] force field implemented therein. Missing ligand parameters were obtained from the implementation of this force field in MacroModel. Two sets of MD simulations were performed, one for the ligands in a 20 Å sphere of TIP3P water (free state) and one for the ligands bound to NTPDase2 where the complex was immersed in a similar sphere (bound state). The surface of the sphere was subjected to radial and polarization restraints according to the SCAAS[48] model as implemented in Q. Nonbonded interactions were calculated for all atoms within the sphere. To avoid overpolarization effects, charged amino acids outside the simulation sphere and within 2−4 Å of the boundary were neutralized. The Ca ion was assigned a charge of +2, and its distances to four crystallographic water molecules and to the chelating oxygens of the ligands were restrained to their initial values. Sodium ions were added to the system to maintain charge neutrality. For the solvated protein−ligand complexes, all atoms outside the 20 Å were tightly restrained to their initial coordinates and excluded from the nonbonded interactions list. While such restraints may prevent large scale interdomain movements known to occur in NTPDases upon ligand binding, the purpose of the LIE simulations was not to describe the binding process but rather the binding of ligands to a preformed site. Furthermore, because of the high similarity between the different analogues considered in this work we expect that for all, the binding site adopts a similar conformation. For the free ligand in water, a weak harmonic restraint with a force constant of 10 kcal/mol·Å^2 was applied to the atoms of ligands to keep it near the sphere center. All the systems were heated from 1 to 300 K in four steps followed by 100 ps long equilibration at 300 K. During the heating phase, restraints on heavy atoms within the simulation sphere were applied and gradually reduced to zero.

This was followed by a 3 ns long production run (among the longest production runs reported for LIE calculations with Q). Ligand-surrounding interaction energies were taken as an average over the

dx.doi.org/10.1021/jm401933c | J. Med. Chem. 2014, 57, 5919−5934

Table 1. Stability of Analogues 1−9 to Hydrolysis by Human NTPDases[a]

	hydrolysis (in %) vs control			
compound	NTPDase1	NTPDase2	NTPDase3	NTPDase8
1	44 ± 5.1	11.5 ± 4.2	NT	NT
2	2.3 ± 0.1	2.8 ± 0.1	0.8 ± 0	3.0 ± 0.2
3	73 ± 5.7	38.5 ± 6.2	NT	NT
4	87 ± 3.0	77 ± 1.0	NT	NT
5	74 ± 1.0	73 ± 5.0	NT	NT
6	22 ± 1.0	0 ± 0	2 ± 0.1	20 ± 1.0
7	14 ± 0.7	3 ± 0.6	8 ± 0.4	13 ± 0.6
8	0 ± 0	0 ± 0	4 ± 0.2	2 ± 0.1
9	6 ± 0.3	3 ± 0.2	10 ± 0.6	5 ± 0.2

[a]Each analogue was tested as a substrate for the indicated recombinant human NTPDase and was compared with the activity obtained with ATP which was set as 100% and which corresponded to 680 ± 34, 930 ± 56, 200 ± 36, and 130 ± 10 nmol $P_i \cdot min^{-1} \cdot mg\ protein^{-1}$ for NTPDase1, -2, -3, and -8, respectively. Results are expressed in % ± SD of three independent experiments, each performed in duplicate. NT = not tested.

production phase of the MD trajectory of each complex, and the binding free energy was calculated according to eq 1:

$$\Delta G_{bind} = \alpha(\langle V_{l\text{-}s}^{vdW}\rangle_{bound} - \langle V_{l\text{-}s}^{vdW}\rangle_{free}) + \beta(\langle V_{l\text{-}s}^{el}\rangle_{bound} - \langle V_{l\text{-}s}^{el}\rangle_{free}) \quad (1)$$

where $V_{l\text{-}s}$ are MD time averages of ligand−solvent (TIP3P water in the free state and protein + TIP3P water in the bound state) nonbonded interactions. The "el" and "vdW" terms refer to electrostatic and van der Waals interactions, respectively. In accord with the original LIE publications,[45] the scaling parameters were set to $\alpha = 0.18$, $\beta = 0.5$. LIE simulations were initiated from the selected poses as described above.

RESULTS

Rational Design of Potential NTPDase Inhibitors. To identify NTPDase inhibitors based on an adenine nucleotide scaffold, we explored the inhibitory effect of adenine nucleotides **1−9** modified at the adenine and 5′-phosphate moieties, Figure 1. Specifically, analogues **4−9** modified at the $N^{6\prime}$,$N^{6\prime\prime}$-position were synthesized to evaluate the recognition of the N^6-region by NTPDases. SAR study of this moiety in adenine nucleotides was triggered by the structure of NTPDase inhibitor ARL 67156.[17] This compound exhibits its inhibitory effect in the micromolar range and is disubstituted at the N^6 position ($N^{6\prime}$,$N^{6\prime\prime}$-diethyl) of the adenine moiety. For this purpose we substituted ATP analogues at the N^6-position by one or two methyl substitutions (analogues **4** and **5**). Furthermore, we compared the inhibitory effect of $N^{6\prime}$,$N^{6\prime\prime}$-disubstituted (Me, Et, or Bz groups) analogues (analogues **5** vs **6** and **7**, respectively). In addition, we studied the effect of the related monophosphate nucleotide analogues **8** and **9** on NTPDase activity. The SAR of the adenine moiety was studied as well with 8-azaadenine nucleotide analogues **1** and **3**, and 2-hexylthioadenine nucleotide analogues **1** and **2**. Finally, the contributaion of Pα,β-nonhydrolyzable bridge to generation of NTPDase inhibitor was evaluated as well, compound **2**.

Synthesis. A series of $N^{6\prime}$,$N^{6\prime\prime}$-disubstituted ATP and AMP analogues, C2-substituted-ATP, or -8-aza-ATP has been synthesized (Scheme 1). 2-Hexylthio-8-aza-ATP analogue, **1**, was synthesized from 2-hexylthio-8-azaadenosine, **10**.[49] Triphosphorylation of **10** using our improved Ludwig's conditions[22] resulted in product **1** in 52% yield (Scheme 1). 2-Hexylthioadenosine 5′-β,γ-methylene triphosphate, **2**, was obtained in 70% yield starting from 2-hexylthioadenosine.[20] 8-Aza-ATP, **3**, was synthesized according to literature methods.[19] 6 -Chloroadenosine-2′,3′,5′-acetate, **13**, was used as a common synthetic intermediate for the preparation of N^6-substituted-adenosine 5′-triphosphate and

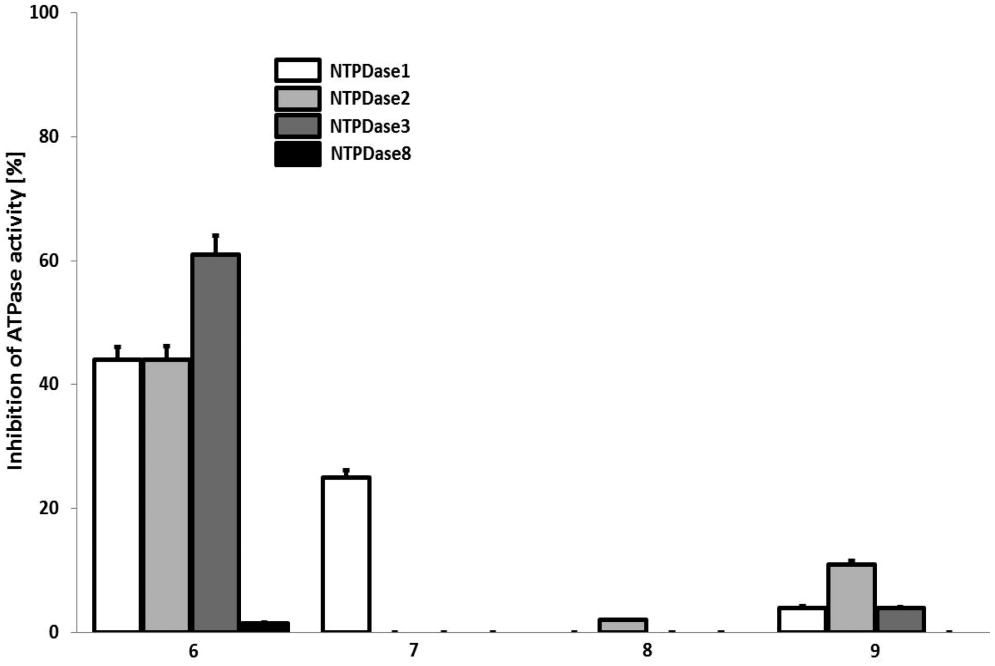

Figure 2. Influence of adenosine nucleotide derivatives **6−9** on recombinant NTPDases activities. Enzymatic assays were carried out using protein extracts from COS-7 cells transfected with an expression vector encoding each enzyme separately. Both substrate and derivatives were used at 100 μM. The 100% activity was set with ATP alone that was 1270 ± 35, 928 ± 55, 202 ± 37, and 129 ± 11 [nmol $P_i \cdot min^{-1} \cdot mg\ protein^{-1}$] for NTPDase1, -2, -3, and -8, respectively. Data are presented as the mean ± SD of three experiments carried out in triplicate.

dx.doi.org/10.1021/jm401933c | J. Med. Chem. 2014, 57, 5919−5934

monophosphate derivatives, **4**–**9** (Scheme 2). $N^{6'}$,$N^{6''}$-Diethyladenosine, **6**, was obtained in 27% yield from **13** by treatment with diethylamine in DMF at 70 °C for 24 h in a sealed tube. These conditions also resulted in the removal of the ribose protecting groups. Similarly, $N^{6'}$,$N^{6''}$-dibenzyladenosine, **17**, was obtained in 44% yield upon treatment of **13** with dibenzylamine. N^6-Methyl- and $N^{6'}$,$N^{6''}$-dimethyladenosine 5′-triphosphate, **4** and **5**, were prepared as we previously reported (Scheme 2).[50] $N^{6'}$,$N^{6''}$-Dimethyladenosine 5′-monophosphate, **8**, was obtained as a byproduct of the triphosphorylation reaction of $N^{6'}$,$N^{6''}$-dimethyladenosine. Compounds **8** and **9** were obtained in 73% and 68% yield, respectively, from $N^{6'}$,$N^{6''}$-dimethyladenosine and $N^{6'}$,$N^{6''}$-diethyladenosine (Scheme 2).[51]

Effect of Nucleotide Derivatives on Recombinant Ectonucleotidase Activity. As described in Experimental Section the protein extracts of nontransfected COS-7 cells showed less than 5% of the activity obtained with COS-7 cells transfected with each ectonucleotidase (NTPDases, ecto-5′-nucleotidase, and NPPs), thus allowing the analysis of each ectonucleotidase in its native membrane-bound form. Previous work demonstrated that NTPDase1 and NTPDase2 possess similar ATPase molecular activity.[52] In our assays here we had a similar level of ATPase activities of both NTPDase1 and NTPDase2, suggesting that similar levels of each NTPDase were used. Western blot confirmed the expression of each protein (data not shown).

Out of the nine analogues studied here, analogues **2**, **6**, **7**, **8**, **9** were reasonably stable to hydrolysis by human NTPDase1–3 and -8 (Table 1). However, the ATPase activity assays performed with equal concentrations (100 μM) of ATP and these analogues revealed that $N^{6'}$,$N^{6''}$-diethyladenosine, **6** (Figure 2), and 2-hexylthio-β,γ-CH_2-ATP, **2** (Figure 3A) inhibited NTPDase2 (about 40% and 70%, respectively) while the other three analogues were either extremely weak inhibitors of NTPDase2 (**7** and **9**) or did not inhibit it (**8**) (Figure 2). 2-Hexylthio-β,γ-CH_2-ATP inhibited human NPP1 activity by >50% (Figure 3B). The enzymatic activity of human ecto-5′-nucleotidase was barely affected by compound **2** (10% inhibition of AMPase activity).

Kinetic analysis was performed only for compound **2**, which exhibited the best inhibitor characteristics. We have tested the kinetic parameters (K_i and IC_{50}) of NTPDase2 inhibition with ATP as substrate. The inhibition constant (K_i) was evaluated to be 21 μM, while the IC_{50} was 40 μM. Cornish–Bowden plot analyses showed a mixed-type inhibition which was mainly competitive (Figure 4A,B) and therefore partly reversible.

Homology Modeling. To create a predictive tool for the design of novel NTPDase2 inhibitors, we studied the two most potent and the two least active analogues in this work (analogues **2**, **6**, **7**, and **9**), as well as several other NTPDase1 inhibitors recently reported by us and also tested for NTPDase2 inhibition (analogues **18**, **19**, **20**; Figure 5).[17] A model of human NTPDase2 was generated based on the X-ray crystal structure of rat NTPDase2 (3CJA)[37] (Figure 6). The model was found to have good stereochemical quality (99.5% of residues residing in the most favored and additional favored regions of the Ramachandran plot and an overall G-factor of −0.05) and a Prosa profile similar to that of the crystal structure of the template (Figure S1, Supporting Information). The template/target main chain RMSD was found to be 0.48 Å, suggesting that the model has the correct NTPDase2 topology. The structure of the model is consistent with the nucleotide binding pattern of NTPDase2 and its proposed catalytic mechanism.[34] The catalytic binding site in the NTPDase2 model contains one calcium ion, which is coordinated by four water molecules and two phosphate oxygens of the ligand (Figure 6C). The adenine base forms a π–π interaction with Tyr350 and a π–cation interaction with Arg394. The 3′ hydroxyl group is hydrogen bonded to Arg245. Several hydrogen bonds are formed between the phosphate chain and the backbone amides or side chains of several residues: Ser48, Ser49, His50, Thr122, Gly204, Ala205, and Ser206 (Table S1, Supporting Information).

To identify structural factors which may contribute to ligand selectivity, a homology model of human NTPDase1 was generated. The selection of template for this model merits some discussion. Three crystal structures of NTPDase1 are currently available in the PDB, namely rat (3ZX0),[53] *Legionella pneumophila* (4BRA)[54]

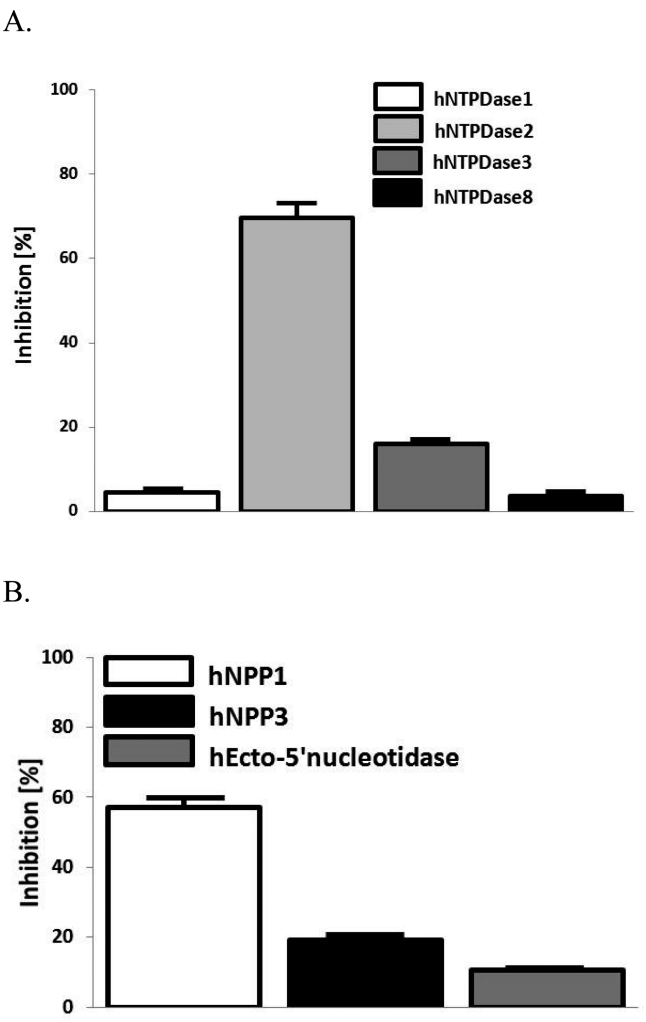

Figure 3. Influence of 2-hexylthio-β,γ-CH_2-ATP, **2**, on recombinant ectonucleotidase activities. Enzymatic assays were carried out with protein extracts from COS-7 cells transfected with an expression vector encoding each enzyme separately. All substrates (ATP, AMP, or pNP-TMP) and **2** were used at 100 μM. For all panels, data are presented as the mean ± SD of three experiments carried out in triplicate. (A) 100% Activity was set with ATP alone: 1270 ± 35; 928 ± 55; 202 ± 37; 129 ± 11 [nmol P_i·min^{-1}·mg $protein^{-1}$] for human NTPDase1, -2, -3, and -8, respectively. (B) The activity of human NPP1 and NPP3 with pNP-TMP as substrate and human ecto-5′-nucleotidase with AMP as substrate in the absence of compound **2** was set as 100% of activity, which was 30 ± 2 and 61 ± 4 [nmol *p*-nitrophenol·min^{-1}·mg $protein^{-1}$] for NPP1 and NPP3, respectively, and 1010 ± 33 [nmol P_i·min^{-1}·mg $protein^{-1}$] for human ecto-5′-nucleotidase.

dx.doi.org/10.1021/jm401933c | J. Med. Chem. 2014, 57, 5919–5934

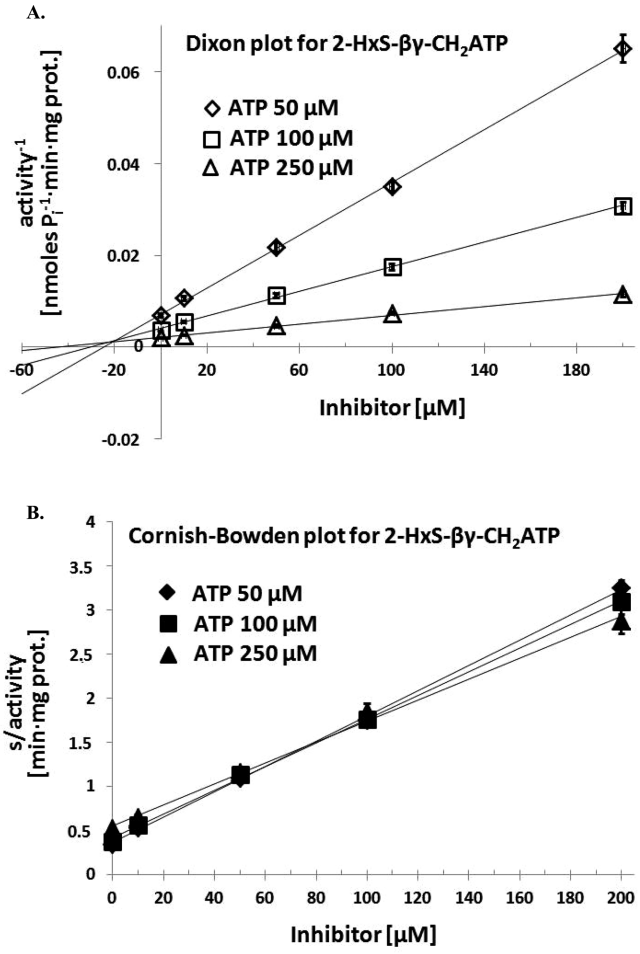

Figure 4. K_i determination for 2-hexylthio-β,γ-CH_2-ATP, **2**, by Dixon (A) and Cornish–Bowden (B) plot. ATP concentration was 50, 100, and 250 μM, in the presence of 0, 10, 50, 100, and 250 μM compound **2**. Data are presented as the mean ± SD of three experiments carried out in triplicate.

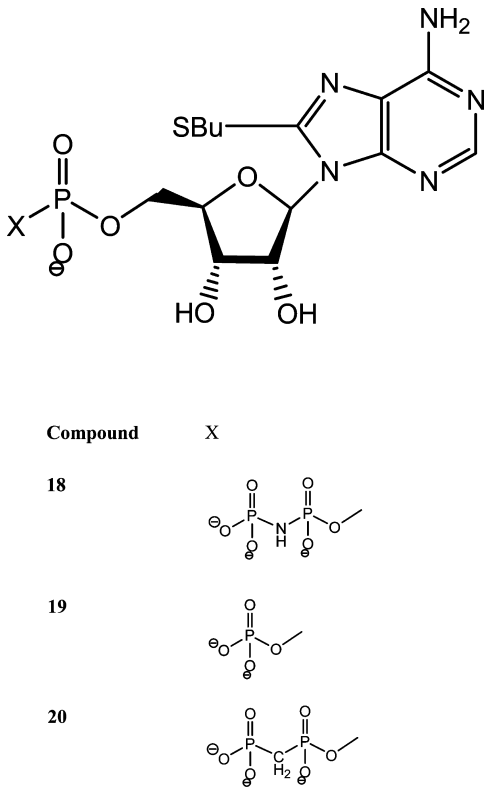

Figure 5. Structures of 8-BuS-ATP and 8-BuS-ADP derivatives, **18**–**20**, which were originally reported in ref 18 and which were subjected to docking and LIE simulations in this study.

and *Toxoplasma gondii* (4KH6). The rat NTPDase structure shares the highest sequence identity with the human protein (73%), yet it was solved in the absence of a nucleotide analogue. The *Legionella pneumophila* and *Toxoplasma gondii* structures were solved in the presence of a metal cofactor and a nucleotide analogue (AMPNP and AMPPNP for *Legionella pneumophila* and *Toxoplasma gondii*, respectively), yet they share a much lower sequence identity with human NTPDase1 (25% and 18% for *Legionella pneumophila* and *Toxoplasma gondii*, respectively). An initial attempt to build a model for human NTPDase1 based on the *Legionella pneumophila* structure resulted in a model with a poor stereochemical quality, presumably due to the low template-target sequence identity. A second attempt at model construction was performed based on the rat NTPDase1 template. However, docking of analogue **2** into this model resulted in an orientation of the triphosphate chain different from that observed in the *Legionella pneumophila* NTPDase1 or in rat NTPDase2 structures. This is likely the consequence of differences in side-chain conformations between the binding sites due to the absence of ligand in the rat NTPDase structure. Thus, we chose to construct a model of human NTPDase1 based on the structure of rat NTPDase2 which, as discussed above, was solved in the presence of a Ca^{2+} cofactor and a relevant ligand (AMPPNP). The resulting model was found to have good stereochemical quality (98.5% of residues residing in the most favored and additional favored regions of the Ramachndran plot and an overall G-factor of −0.1), a Prosa profile similar to that of the crystal structure of the template (Figure S1, Supporting Information), and a template/target main chain RMSD value of 0.62 Å. A sequence and structural comparison between the two models is presented in Figure 7. Both models have very similar binding sites with residues forming stabilizing interactions with the crystallographic ligand (AMPPNP) in NTPDase2 highly conserved in NTPDase1 (residues Ser48, Ser49, His50, Thr122, and Ala205 in NTPDase2 correspond, respectively, to residues Ser57, Ser58, His59, Thr131, and Ala217 in NTPDase1; see Table S1, Supporting Information), yet they differ by several residues both within and in close vicinity to the site. In particular, Arg245, Tyr350, Asp353, and Arg394 in NTPDase2 are respectively replaced by Lys258, Phe365, Lys368, and Tyr408 in NTPDase1. While the first two changes are conservative (Arg → Lys, Tyr → Phe), the last two may affect ligand binding and form the basis for ligand selectivity.

Docking Simulations. Docking simulations for all ligands were initiated from conformational ensembles generated by the conformational search procedure. This approach provides the docking tool with multiple starting points including different ring conformations. Docking simulations with Glide successfully reproduced the crystallographic pose (i.e., binding mode) of AMPPNP in the rat NTPDase2 binding site as the lowest energy structure with an heavy atoms RMSD of 0.61 Å (data not shown).

Encouraged by these results, NTPDase2 inhibitors and related molecules (analogues **2**, **6**, **7**, **9**, **18**, **19**, **20**; Figures 1 and 6) were docked into the binding site of the human NTPDase2 model. All analogues occupied the catalytic binding site forming

dx.doi.org/10.1021/jm401933c | J. Med. Chem. 2014, 57, 5919–5934

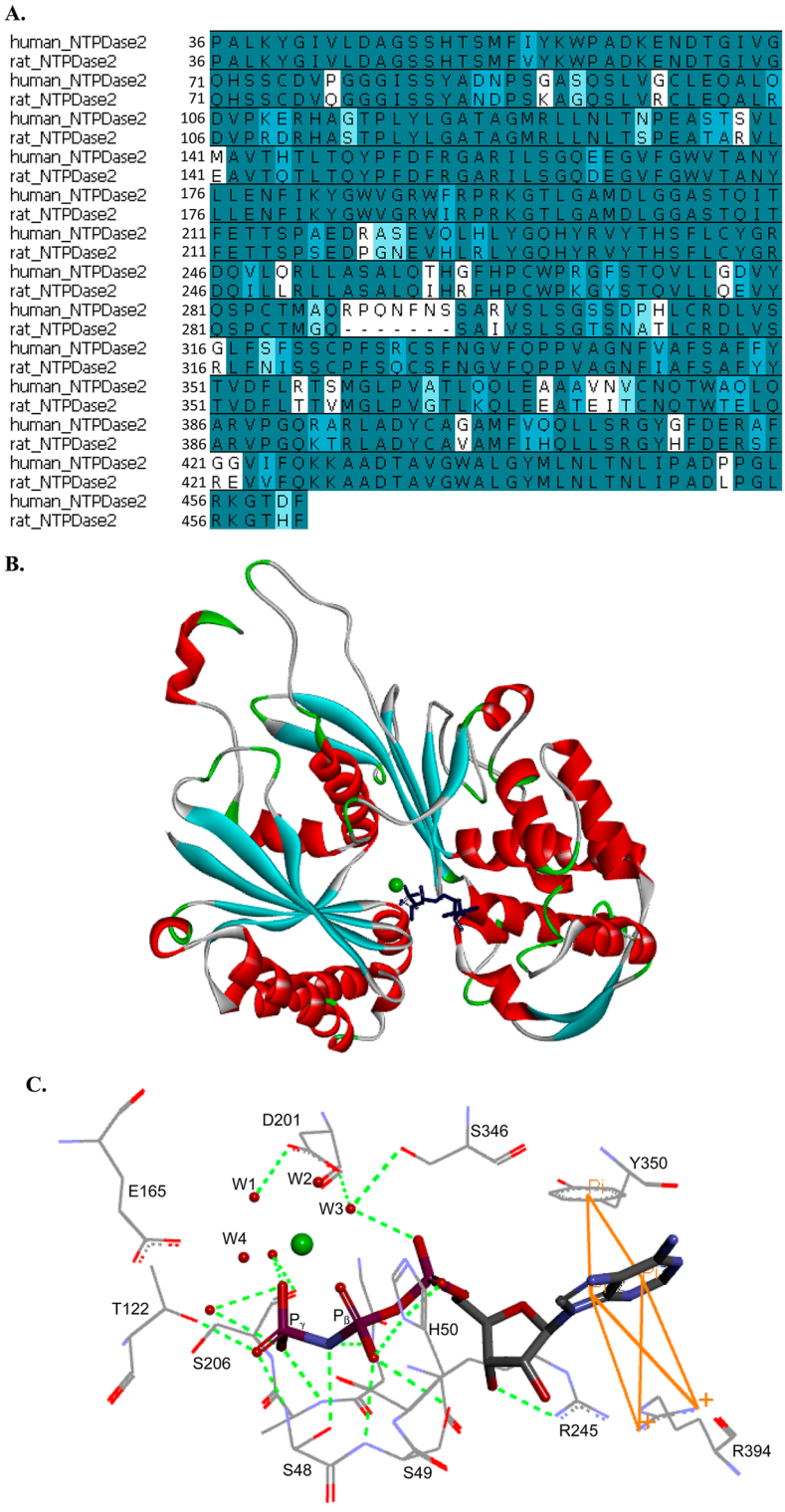

Figure 6. Homology model of human NTPDase2. A: Sequence alignment of human NTPDase2 and rat NTPDase2 (3CJA). Identical, similar, and nonsimilar residues are depicted in dark blue, light blue, and white, respectively. B: 3D model of human NTPDase2 with AMPPNP in its catalytic site. The protein is shown as a ribbon diagram color coded according to its secondary structure, the Ca^{2+} ion is shown in green, and the AMPPNP molecule is depicted in blue. C: 3D model of the catalytic site of human NTPDase2 highlighting the interactions between AMPPNP and binding site residues. The Ca^{2+} ion is shown as a green sphere, the six conserved water molecules are represented by red spheres (the water molecules that coordinate the Ca^{2+} ion are W1−W4), and the AMPPNP molecule is colored according to atom types (nitrogen atoms in blue, oxygen atoms in red, carbon atoms in gray, phosphate atoms in purple). Hydrogen bonds and $\pi-\pi$ and $\pi-$cation interactions are shown in green and orange, respectively.

interactions with binding site residues similar to those formed by AMPPNP, suggesting that, in principle, they could compete with the endogenous ligand (ATP) for binding site interactions. Analogues however differ in the relative orientations of the ribose and base moieties. Analogues with substitution at the C8 position (analogues **18**, **19**, **20**) adopt a syn conformation

dx.doi.org/10.1021/jm401933c | *J. Med. Chem.* 2014, 57, 5919−5934

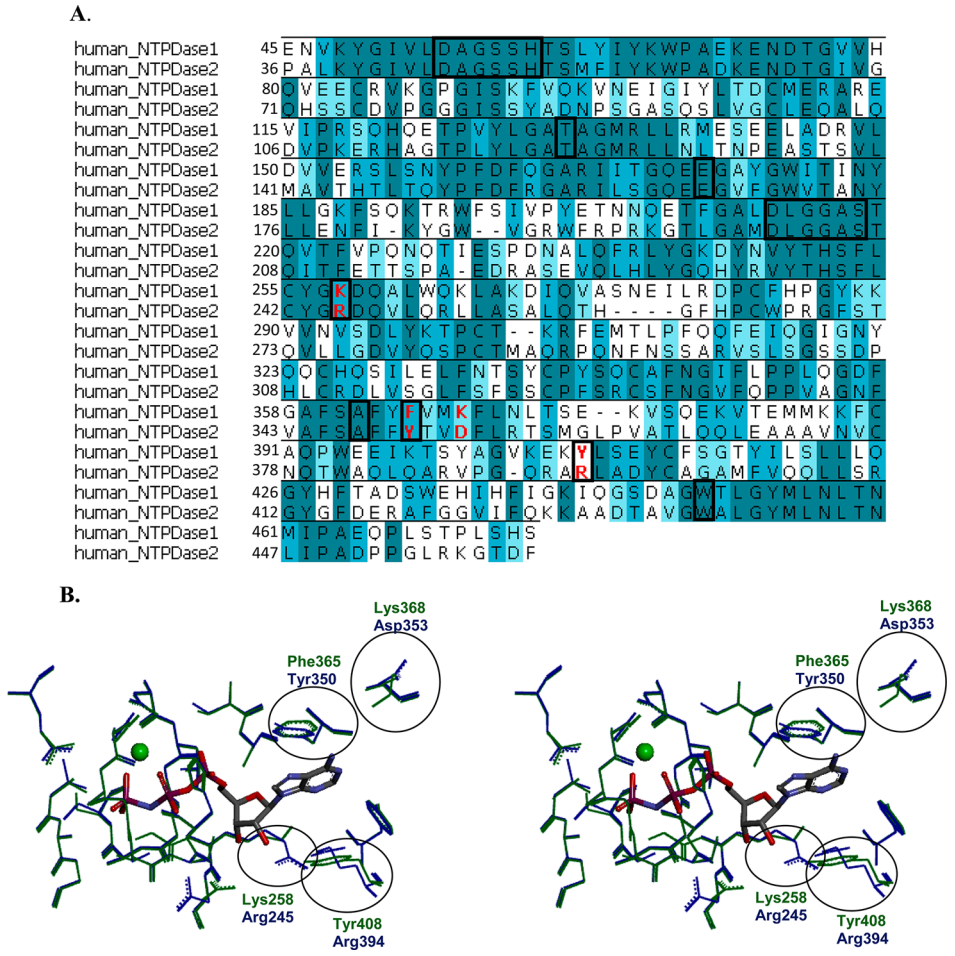

Figure 7. A comparison between NTPDase2 and NTPDase1 homology models. (A) Sequence alignment between human NTPDase1 and NTPDase2. The overall sequence identity is 41.4%. The sequence identity between binding sites residues (boxed regions) is 84.2%. Different residues in both the binding site and in close vicinity to it are bolded in red. (B) Superposition of the binding sites of human NTPDase2 (blue) and NTPDase1 (green). The corresponding pairs Lys258 on NTPDase 1 vs Arg245 on NTPDase2, Phe365 on NTPDase1 vs Tyr350 on NTPDase2, Lys368 on NTPDase1 vs Asp353 on NTPDase2, and Tyr408 on NTPDase1 vs Arg394 on NTPDase2 are circled.

whereas analogues lacking such substitutions (**2**, **6**, 7, **9**) adopt an anti conformation.[20] To obtain insight into the origin of the inhibitory activity, an attempt was made to correlate the docking scores for all analogues with their % inhibition values. This attempt however was unsuccessful (data not shown). Similarly, a detailed interaction analysis for all analogues (see Table S1, Supporting Information) failed to reveal the source of their differential activities.

LIE Simulations. Assuming that the efficacy of the highly charged and flexible ATP analogues considered in this work depends on factors not accounted for by docking simulations, for example, desolvation energies and entropy penalties, we turned our attention to MD simulations using the linear interaction energy (LIE) approach.[51,52] Simulations were initiated from the lowest energy poses and from the AMPPNP-like poses of analogues **2**, **6**, 7, **9**, **18**, **19**, and **20** (Figure 8 and Table S1, Supporting Information), yet only the latter poses provided good correlation with the experimental binding free energy data and will be further discussed. Table 2 lists the individual energy components obtained from the LIE simulations as well as the computed binding free energies (ΔG_{LIE}). In terms of the van der Waals energies, all ligands preferred the protein over the water environment (the $\langle V_{l\text{-}s}^{vdW}\rangle_p$ term which describes the averaged ligand−protein vdW energy was always lower than the $\langle V_{l\text{-}s}^{vdW}\rangle_w$ which describes the averaged ligand−water vdW energy). In terms of the electrostatic energy, only analogue **2** (the most active compound) preferred the protein over the water environment (the $\langle V_{l\text{-}s}^{el}\rangle_p$ term which describes the averaged ligand−protein electrostatic energy was lower than the $\langle V_{l\text{-}s}^{el}\rangle_w$ which describes the averaged ligand−water electrostatic energy for analogue **2** only and higher for all other analogues). These data suggest that improving the inhibition potency of NTPDase2 inhibitors may require further optimization of their electrostatic interactions with the bind site. The correlations between the LIE-based binding free energies and the experimental % inhibition data for the triphosphate, triphosphate diphosphate, and for all analogues studied in this work are presented in Figure 9, parts a, b, and c, respectively. In contrast with the poor results obtained with the docking simulations (see above), these good correlations (r^2 = 0.94, r^2 = 0.86, and r^2 = 0.68) lend credit to our hypothesis concerning the need to use a proper treatment of molecular flexibility and solvation effects for the accurate prediction of binding of ATP analogues to NTPDase2.

Docking Simulations at NTPDase1. To gain insight into the structural factors governing NTPDase2/NTPDase1 selectivity, analogue **2**, the most active and selective compound discovered in this work, was docked into the catalytic site of the

dx.doi.org/10.1021/jm401933c | J. Med. Chem. 2014, 57, 5919−5934

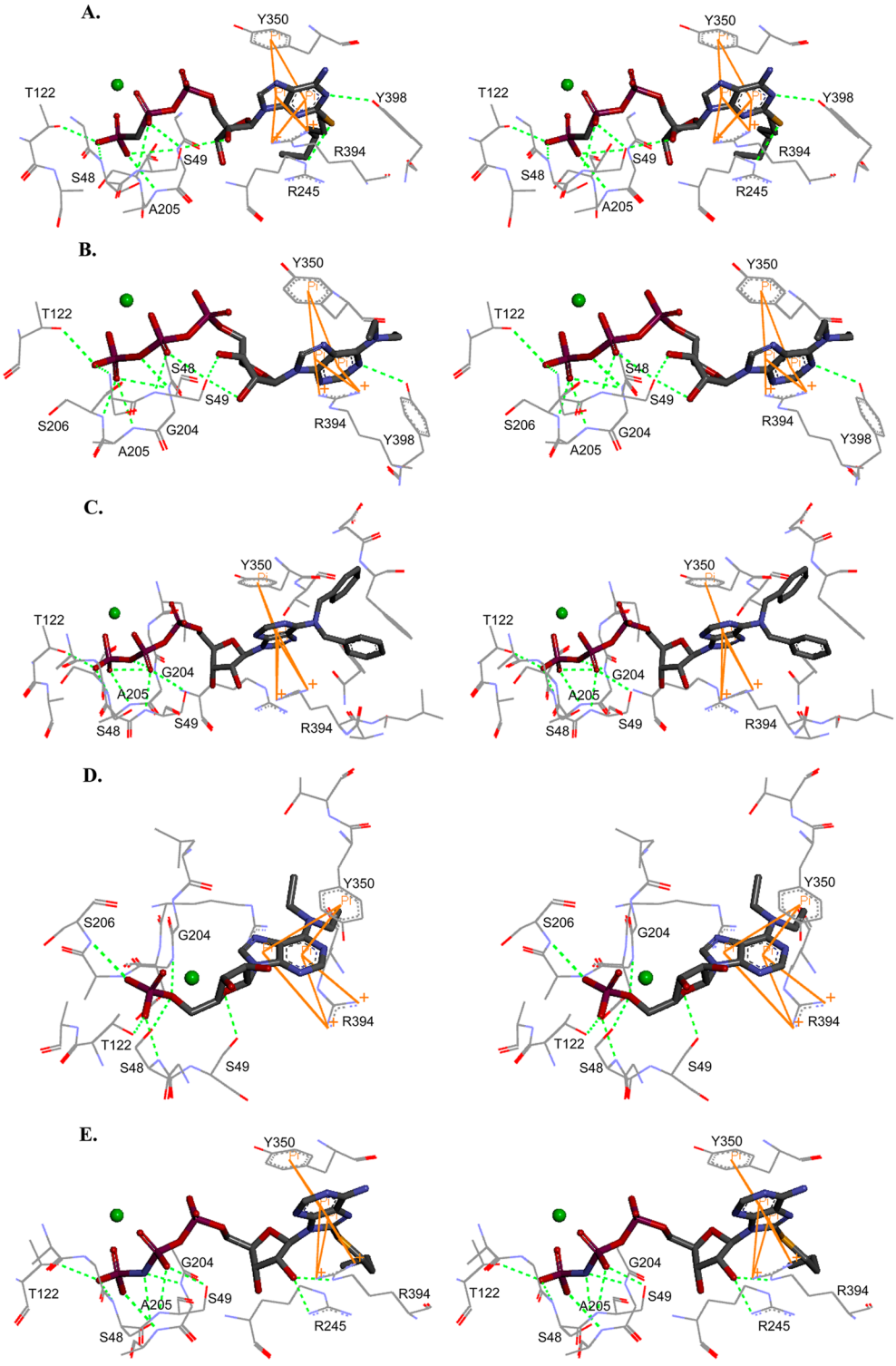

Figure 8. Starting points for LIE simulations. Panels A–G present the starting points for the LIE simulations for ligands **2**, **6**, **7**, **9**, **18**, **19**, and **20**, respectively. The Ca^{2+} ion is shown as a green sphere, the six conserved water molecules are represented by red spheres, and the ligands are colored according to atom types (nitrogen atoms in blue; oxygen atoms in red; carbon atoms in gray; phosphate atoms in purple). Hydrogen bonds and $\pi-\pi$ and $\pi-$cation interactions are shown in green and orange, respectively. Panel H presents the superimposition of the starting points for all analogues **2** (green), **6** (yellow), **7** (purple), **9** (orange), **18** (red), **19** (cyan), **20** (magenta), and the crystal AMPPNP (blue).

human NTPDase1 model. Figure 10 provides a comparison between representative binding modes of analogue **2** in the catalytic sites of the two enzyme models. In NTPDase2, the adenine ring is tightly stacked between Tyr350 and Arg394, forming $\pi-\pi$ and $\pi-$cation interactions, respectively ($R_{\text{adenine-Tyr350}}$ = 4.19 Å; $R_{\text{adenine-Arg394}}$ = 4.38 Å). In NTPDase1, Arg394 is replaced by Tyr408, leading to a loss of a $\pi-$cation interaction and to a potential gain of a $\pi-\pi$ interaction. However, the aromatic ring of Tyr408 is too remote from the adenine ring of the inhibitor, **2**, to effectively interact with it

dx.doi.org/10.1021/jm401933c | J. Med. Chem. 2014, 57, 5919–5934

Table 2. Calculated Binding Energies (kcal/mol) and % Inhibition for Analogues 2, 6, 7, 9, 18, 19, and 20 Using the LIE Approach[a]

compound	percent of inhibition	$\langle V_{l\text{-}s}^{vdW}\rangle_w$	$\langle V_{l\text{-}s}^{el}\rangle_w$	$\langle V_{l\text{-}s}^{vdW}\rangle_p$	$\langle V_{l\text{-}s}^{el}\rangle_p$	ΔG_{LIE}
2	70	10.0 ± 0.6	−1640 ± 10	−29.6 ± 0.6	−1647 ± 7	−10.4
6	42	11.3 ± 0.9	−1653 ± 15	−25.6 ± 1.0	−1621 ± 11	9.3
7	0	0.9 ± 0.5	−1686 ± 13	−31.9 ± 4.1	−1583 ± 3	45.4
9	10	−6.7 ± 0.4	−588.6 ± 6.3	−29.5 ± 0.9	−563 ± 8	8.7
18	30	13.1 ± 0.4	−1668 ± 14	−31.1 ± 1.6	−1631 ± 6	10.4
19	18	2.2 ± 0.4	−1097 ± 5.5	−36.1 ± 0.4	−1057 ± 4	13.0
20	18	14.7 ± 0.8	−1710 ± 21	−30.6 ± 1.9	−1648 ± 11	22.9

[a]The $V_{l\text{-}s}$ terms represent MD time averages of analogue−solvent nonbonded interactions where solvent is taken as TIP3P water for the free state and the protein immersed in TIP3P water for the bound state. The "el" and "vdW" terms refer to electrostatic and van der Waals interactions, respectively. The coefficients α and β take the values of 0.18 and 0.5, respectively.

($R_{adenine\text{-}Tyr408}$ = 5.52 Å). This leads to a shift in the position of the adenine ring and to a concomitant change in the position of the thiohexyl chain. Thus, while in NTPDase2 this chain is deeply buried within a hydrophobic pocket within the binding site, in NTPDase1, it is much more exposed to the solvent. We therefore propose that the unfavorable exposure of a hydrophobic part of analogue **2** to the solvent in NTPDase1 is at least partially responsible for its selectivity toward NTPDase2.

DISCUSSION

NTPDase2 has been detected on blood vessels,[55] cultured brain astrocytes,[56] neuronal progenitor,[57] and in cancer cells.[58,59] Thus, NTPDase2 can potentially be the target for novel drugs for the treatment of cancer and cardiovascular or central nervous system disorders. Potent and selective NTPDase2 inhibitors are therefore required. With this in mind, we have studied C2- and N^6-substituted ATP derivatives. Nucleotides with modified $N^{6'}$,$N^{6''}$-position were synthesized to evaluate the tolerance of NTPDases to the presence of N^6-methyl, -ethyl, or -benzyl groups (compounds **4**−**9**). The SAR of the adenine C8- and C2-positions was studied as well by 8-azaadenine nucleotide analogues **1** and **3**, and 2-thiohexyl nucleotide analogues, **1** and **2**.

First, nucleotide derivatives **4**−**9** were studied as NTPDases substrates. $N^{6'}$,$N^{6''}$-Methyl- and dimethyl-substituted ATP derivatives **4** and **5** were hydrolyzed to ca. 80% by all NTPDases, while compounds **6**−**9** were only modest substrates (Table 1). The latter compounds were therefore further tested as NTPDase inhibitors (Figure 2). Compounds **7**−**9** did not inhibit NTPDases, while $N^{6'}$,$N^{6''}$-diethyl-ATP, **6**, had a modest nonspecific inhibitory effect on all tested NTPDases, similar to the closely related ARL 67156.[17]A bulkier substitution (dibenzyl) makes the compound **7** nonactive both as substrate and inhibitor, showing that NTPDase2 is tolerant to Me or Et groups but is not tolerant to steric hindrance by two benzyl groups at the N^6-position.

2-Hexthio-8-aza-ATP, **1**, substituted at both C2 and 8 positions, was hydrolyzed by NTPDase1 and NTPDase2 in about 40% and 10%, respectively. To isolate the effect of the 8-aza or 2-hexylthio group on recognition and subtype selectivity, we synthesized and evaluated two additional compounds: 8-aza-ATP, **3**, and 2-hexylthio-β,γ-CH_2-ATP, **2**. Compound **3** was hydrolyzed by both NTPDase1 and -2, indicating that the 2-hexylthio group of **1** provided resistance to hydrolysis by NTPDase2. As expected, compound **2** was not hydrolyzed by NTPDases1−3 and -8. Furthermore, it proved to be an effective NTPDase2 inhibitor (K_i = 21 μM). Compound **2** was the most selective inhibitor tested here, inhibiting (at 100 μM) NTPDase2, NTPDase1, NTPDase3, and NTPDase8 by 70%, <10%, ∼15%, and <10%, respectively (Figure 3A). It did not affect the activity of ecto-5′-nucleotidase and partially inhibited human NPP1 (Figure 3C). Kinetic analysis using the Dixon[32] and Cornish−Bowden method[32,60] revealed that compound **2** displayed a mixed-type, predominantly competitive, inhibition toward recombinant human NTPDase2 (Figure 4 A,B). Interestingly, ATP-β,γ-CH_2 does not decrease the ATPase activity of NTPDase2[34,61] and, in this light, substitution at the C2 position by a thiohexyl group seems to be crucial for this inhibition.

The kinetic parameters of analogue **2** were found to be superior to those of the nonspecific inhibitors ARL 67156 and (PSB-6426).[18] The potency of compound **2** (K_i = 21 μM) is of the same order as that of PSB-6426, (K_i = 8.2 μM), but the selectivity of **2** toward NTPDase2 vs NTPDase1 was better than that of PSB-6426. The latter inhibited NTPDase1 by 50% at the same concentration it fully inhibited NTPDase2.

The importance of developing potent and selective NTPDase2 inhibitors, and not only general NTPDase inhibitors, is highlighted by the opposite effects of NTPDase1 and NTPDase2 on platelet aggregation. NTPDase1 hydrolyzes both ATP and ADP, whereas NTPDase2 is a preferential nucleoside triphosphatase-hydrolyzing enzyme. Thus, by hydrolyzing ADP, which is an aggregation factor, NTPDase1 inhibits platelet aggregation, while in contrast, NTPDase2 promotes platelet aggregation in the presence of ATP. Differential cellular expression of NTPDases in the vasculature suggests a spatial regulation of nucleotide-mediated signaling. In this context, NTPDase1 should abrogate platelet aggregation and recruitment in intact vessels by the conversion of ADP to adenosine monophosphate, while NTPDase2 expression would promote platelet microthrombus formation at sites of extravasation following vessel injury. Thus, selectivity of the inhibitor toward these two enzymes is critical.

To provide structural insight into the activities of NTPDase2 inhibitors, a ligand-supported homology model of the protein was generated based on the high resolution crystal structure of rat NTPDase2.[34] Docking simulations using Glide successfully reproduced the crystallographic pose of AMPPNP within the rat NTPDase2 binding site (heavy atoms RMSD of 0.61 Å). Encouraged by these results, compounds **2**, **6**, **7**, **9**, **18**, **19**, and **20** were docked into the binding site of the model, yet attempts to correlate the docking scores or the interaction patterns with % inhibition data have proven unsuccessful. Assuming that this lack of correlation results from factors not accounted for by docking simulations such as desolvation energies and entropy penalties, we have turned our efforts to LIE simulations.[44,45]

dx.doi.org/10.1021/jm401933c | J. Med. Chem. 2014, 57, 5919−5934

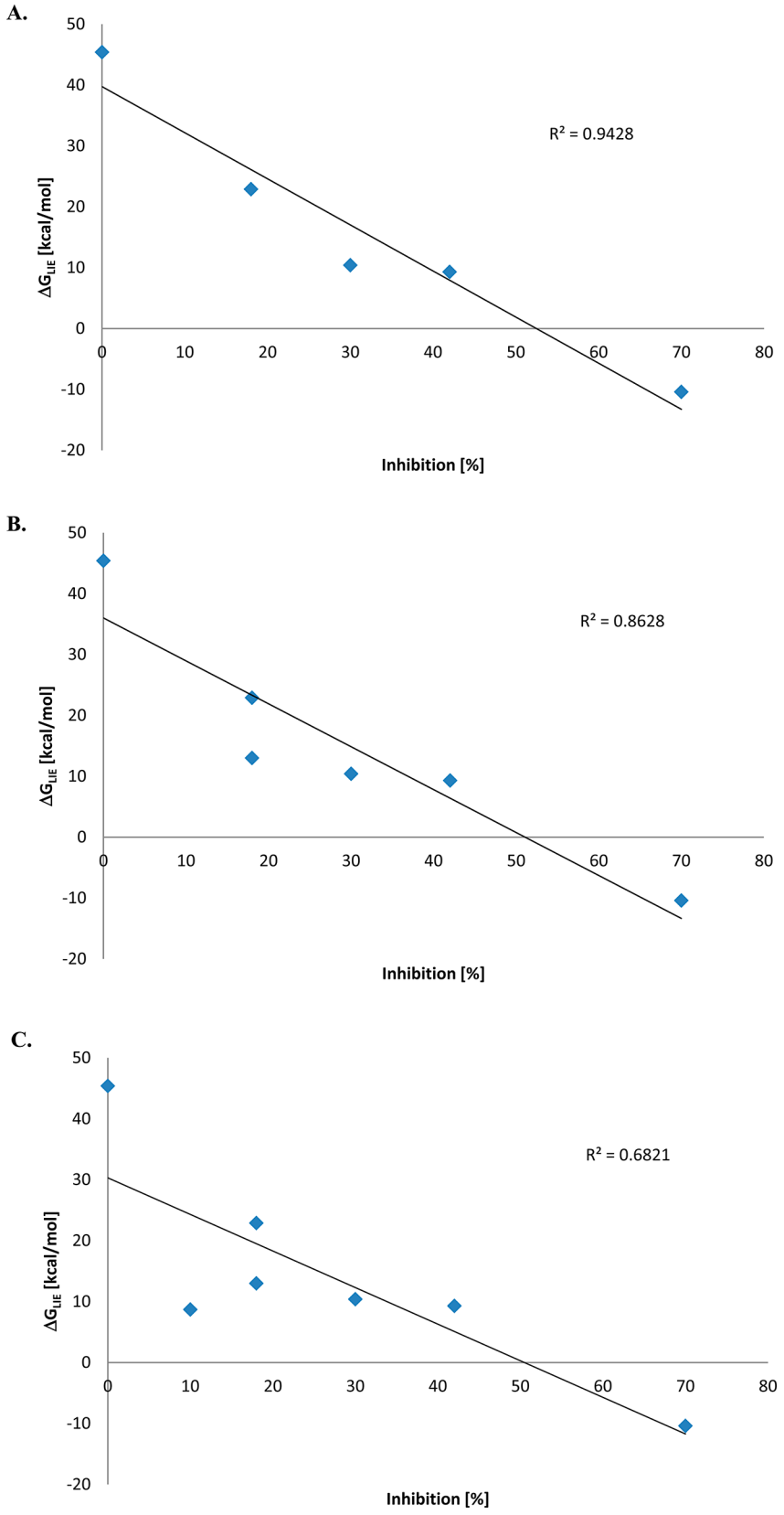

Figure 9. Correlation between calculated free energy of binding and % inhibition. Correlation between binding free energies calculated using the LIE approach and experimentally determined % inhibition for (A) the triphosphate analogues **2**, **6**, **7**, **18**, and **20**, (B) the triposphate and diphospate analogues (**2**, **6**, **7**, **18**, **19**, **20**), and (C) all analogues. % Inhibition for the inactive analogue **7** was set to zero.

Indeed, when initiated from AMPPNP-like (but not from lowest energy; results not shown) poses, these simulations provided a very good correlation between experiment (% inhibition) and calculations. This correlation is particularly good when considering only the triphosphate analogues (analogues **2**, **6**, **7**, **18**, **20**; r^2 = 0.94; Figure 9a) and slightly decreases when

dx.doi.org/10.1021/jm401933c | J. Med. Chem. 2014, 57, 5919−5934

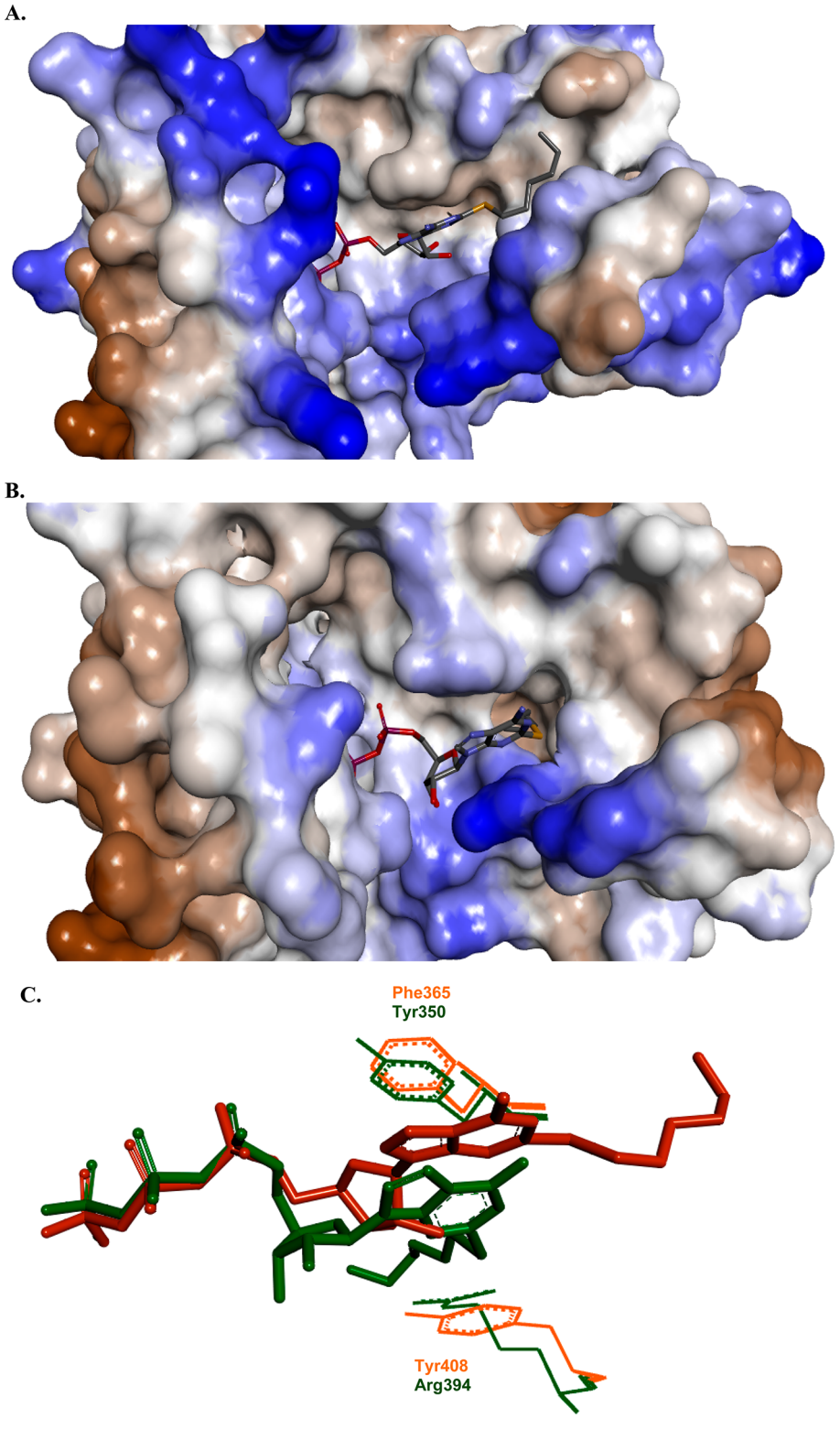

Figure 10. A comparison of representative binding modes of analogue **2** in the catalytic site of the human NTPDase2 and NTPDase1 homology models. (A) Surface of the human NTPDase1 model colored according to its hydrophobicity (hydrophilic and hydrophobic regions colored in blue and brown, respectively). (B) Surface of the human NTPDase2 model colored according to its hydrophobicity (color coding as in A). (C) Superposition of representative poses of analogue **2** in the catalytic site of NTPDase2 (green) and NTPDase1 (orange). Also shown are key residues which interact with the adenine ring (NTPDase2: Tyr350 and Arg394 colored in green; NTPDase1: Phe365 and Arg394 colored in orange). The different position of the adenine rings in the two sites is clearly visible.

including the diphosphate analogue (**19**; r^2 = 0.86; Figure 9b) and the monophsphate analogue (**9**, r^2 = 0.68; Figure 9c). Indeed, LIE simulations work best for congeneric series.[62]

Table 2 demonstrates the expected trend between the formal charges of the analogues and their electrostatic energies, both in solution and in the protein environment. Thus, the average

dx.doi.org/10.1021/jm401933c | J. Med. Chem. 2014, 57, 5919−5934

electrostatic energy for the triphosphate analogues (**2**, **6**, **7**, **18**, **20**; formal charge (−4)) is −1671 (solution) and −1626 (protein) kcal/mol, that of the diphosphate analogue (**19**, formal charge (−3)) is −1097 (solution) and −1057 (protein) kcal/mol and that of the monophosphate analogue (**9**, formal charge (−2)) is −588 (solution) and −563 (protein) kcal/mol. From all analogues, only analogue **2** has a negative ΔV_{el} ($= \langle V_{l\text{-}s}^{el} \rangle_p - \langle V_{l\text{-}s}^{el} \rangle_w$) term, while for the rest of the ligands this term is positive. Thus, this is the only ligand which prefers the protein over the solvent environment in terms of electrostatic interactions. Furthermore, the least potent analogue, **7**, has the largest electrostatic preference for solution (ΔV_{el} = 103 kcal/mol). Controlling the protein/solvent electrostatic interactions balance may therefore be key to the design of more efficacious NTPDase2 inhibitors. For example, replacement of any polar moiety within a ligand which favors the solvent over the protein by a nonpolar group may improve binding by reducing the desolvation penalty. While an atom by atom analysis of the MD trajectory for analogue **2** revealed that in this case all polar moieties prefer the protein environment, a similar analysis of other ligands may point to modifications which may increase the binding affinity. We therefore propose that the LIE method could be used as a design tool for both predicting ligand−protein electrostatic energies as well as the overall NTPDase2 binding energies of potential NTPDase2 inhibitors.

Given the importance of NTPDase1/2 inhibitor's selectivity, a homology model of NTPDase1 was developed and compared to that of NTPDase2. Both models have highly conserved binding sites, yet they differ by several residues (Figure 7). In particular, Arg245, Tyr350, Asp353, and Arg394 in NTPDase2 are respectively replaced by Lys258, Phe365, Lys368, and Tyr408 in NTPDase1. As shown in Figure 10, these changes result in different interactions of the adenine ring with its "flanking" residues (Tyr350 and Arg394 in NTPDase2 and Phe365 and Tyr408 in NTPDase1) which ultimately lead to an unfavorable shift of the hydrophobic thiohexyl chain from a buried conformation in NTPDase2 to a solvent-exposed conformation in NTPDase1. This may at least partially explain the selectivity of analogue **2** toward NTPDase2.

Finally, the differences between the binding sites of NTPDase1 and 2 could be utilized to confer NTPDase1 or NTPDase2 selectivity by further modifications to the inhibitors described in this study. For example, substituting the C2 position of the adenine ring by a positive- or negative-charge terminated thioalkyl chain, which would interact with Asp353 or Lys368, may lead to selectivity toward NTPDase2 or NTPDase1, respectively (Figure 7). Such design efforts are currently being conducted in our laboratory.

In summary, 2-hexylthio-β,γ-methylene-ATP, **2**, may be used to selectively block NTPDase2 ectonucleotidase activity. Compound **2** may be a good starting point for the development of drugs for the treatment of certain cardiovascular disorders, especially when controlling the ADP level is essential as in atherosclerosis.[40,42] Balancing ADP levels may indeed be important for the therapy of diseases where platelet dysfunction is a key component and also for cancer therapy and cardioprotection. Such development efforts could benefit from the homology models of NTPDase1 and 2 and from the computational models for binding free energy prediction developed in this work.

■ ASSOCIATED CONTENT

Supporting Information

Additional information as noted in text. This material is available free of charge via the Internet at http://pubs.acs.org.

■ AUTHOR INFORMATION

Corresponding Authors

*Tel: 972-3-5318303. Fax: 972-3-6353907. E-mail: bilha.fischer@mail.biu.ac.il.

*Tel: 418-525-4444. Fax: 418-654-2765. E-mail: Jean.Sevigny@crchul.ulaval.ca.

*Tel: 972-3-7384588. Fax: 972-3-7384588. E-mail: hsenderowitz@gmail.com.

Author Contributions

⊥I.G., J.L., and L.S. contributed equally to this work

Notes

The authors declare no competing financial interest.

■ ACKNOWLEDGMENTS

This work was supported by grants from the Heart & Stroke Foundation (HSF) of Quebec and from the Canadian Institutes of Health Research (CIHR; MOP-102472, IRO-102806) to JS. M.F. was the recipient of a Doctoral Scholarship from the Government of Gabon, M.M.-S. of a fellowship from the Spanish Ministry of Education and Science (MEC, Jose Castillejo Program), and J.S. of a senior Scholarship from the Fonds de recherche du Québec − Santé (FRQS).

■ ABBREVIATIONS USED

E-NPP, ecto-nucleotide pyrophosphatase/phosphodiesterase; E-NTPDase, ecto-nucleoside triphosphate diphosphohydrolase; Pi, inorganic phosphate; pnp-TMP, *p*-nitrophenylthymidine 5′-monophosphate; POM, polyoxometalates; TEAA, triethylammonium acetate; TBAP, tetrabutylammonium phosphate

■ REFERENCES

(1) Yegutkin, G. G. Nucleotide- and nucleoside-converting ectoenzymes: Important modulators of purinergic signalling cascade. *Biochim. Biophys. Acta* **2008**, *1783*, 673−694.

(2) Zimmermann, H.; Zebisch, M.; Strater, N. Cellular function and molecular structure of ecto-nucleotidases. *Purinergic Signalling* **2012**, *8*, 437−502.

(3) Kukulski, F.; Lévesque, S. A.; Lavoie, É. G.; Lecka, J.; Bigonnesse, F.; Knowles, A. F.; Robson, S. C.; Kirley, T. L.; Sévigny, J. Comparative hydrolysis of P2 receptor agonists by NTPDases 1, 2, 3 and 8. *Purinergic Signalling* **2005**, *1*, 193−204.

(4) Zimmermann, H. 5′-Nucleotidase: Molecular structure and functional aspects. *Biochem. J.* **1992**, *285*, 345−365.

(5) Iqbal, J.; Jirovsky, D.; Lee, S. Y.; Zimmermann, H.; Müller, C. E. Capillary electrophoresis-based nanoscale assays for monitoring ecto-5′-nucleotidase activity and inhibition in preparations of recombinant enzyme and melanoma cell membranes. *Anal. Biochem.* **2008**, *373*, 129−140.

(6) Strater, N. Ecto-5′-nucleotidase: Structure function relationships. *Purinergic Signalling* **2006**, *2*, 343−350.

(7) Krug, U.; Patzschke, R.; Zebisch, M.; Balbach, J.; Sträter, N. Contribution of the two domains of E. coli 5′-nucleotidase to substrate specificity and catalysis. *FEBS Lett.* **2013**, *587*, 460−466.

(8) Shryock, J. C.; Belardinelli, L. Adenosine and adenosine receptors in the cardiovascular system: Biochemistry, physiology, and pharmacology. *Am. J. Cardiol.* **1997**, *79*, 2−10.

(9) Koszalka, P.; Özüyaman, B.; Huo, Y.; Zernecke, A.; Flögel, U.; Braun, N.; Buchheiser, A.; Decking, U. K. M.; Smith, M. L.; Sévigny, J.; Gear, A.; Weber, A.-A.; Molojavyi, A.; Ding, Z.; Weber, C.; Ley, K.;

Zimmermann, H.; Gödecke, A.; Schrader, J. Targeted disruption of cd73/ecto-5′-nucleotidase alters thromboregulation and augments vascular inflammatory response. *Circ. Res.* **2004**, *95*, 814−821.
(10) Kawashima, Y.; Nagasawa, T.; Ninomiya, H. Contribution of ecto-5′-nucleotidase to the inhibition of platelet aggregation by human endothelial cells. *Blood* **2000**, *96*, 2157−2162.
(11) Wink, M. R.; Braganhol, E.; Tamajusuku, A. S. K.; Lenz, G.; Zerbini, L. F.; Libermann, T. A.; Sévigny, J.; Battastini, A. M. O.; Robson, S. C. Nucleoside triphosphate diphosphohydrolase-2 (NTPDase2/CD39L1) is the dominant ectonucleotidase expressed by rat astrocytes. *Neuroscience* **2006**, *138*, 421−432.
(12) Šali, A.; Blundell, T. L. Comparative protein modelling by satisfaction of spatial restraints. *J. Mol. Biol.* **1993**, *234*, 779−815.
(13) Braganhol, E.; Morrone, F. B.; Bernardi, A.; Huppes, D.; Meurer, L.; Edelweiss, M. I. A.; Lenz, G.; Wink, M. R.; Robson, S. C.; Battastini, A. M. O. Selective NTPDase2 expression modulates in vivo rat glioma growth. *Cancer Sci.* **2009**, *100*, 1434−1442.
(14) Lecka, J.; Gillerman, I.; Fausther, M.; Salem, M.; Munkonda, M. N.; Brosseau, J.-P.; Cadot, C.; Martín-Satué, M.; d'Orléans-Juste, P.; Rousseau, É.; Poirier, D.; Künzli, B.; Fischer, B.; Sévigny, J. 8-BuS-ATP derivatives as specific NTPDase1 inhibitors. *Br. J. Pharmacol.* **2013**, *169*, 179−196.
(15) Müller, C. E.; Iqbal, J.; Baqi, Y.; Zimmermann, H.; Röllich, A.; Stephan, H. Polyoxometalates-a new class of potent ecto-nucleoside triphosphate diphosphohydrolase (NTPDase) inhibitors. *Bioorg. Med. Chem. Lett.* **2006**, *16*, 5943−5947.
(16) Crack, B. E.; Pollard, C. E.; Beukers, M. W.; Roberts, S. M.; Hunt, S. F.; Ingall, A. H.; McKechnie, K. C.; IJzerman, A. P.; Leff, P. Pharmacological and biochemical analysis of FPL 67156, a novel, selective inhibitor of ecto-ATPase. *Br. J. Pharmacol.* **1995**, *114*, 475−481.
(17) Lévesque, S. A.; Lavoie, E. G.; Lecka, J.; Bigonnesse, F.; Sévigny, J. Specificity of the ecto-ATPase inhibitor ARL 67156 on human and mouse ectonucleotidases. *Br. J. Pharmacol.* **2007**, *152*, 141−150.
(18) Brunschweiger, A.; Iqbal, J.; Umbach, F.; Scheiff, A. B.; Munkonda, M. N.; Sévigny, J.; Knowles, A. F.; Müller, C. E. Selective nucleoside triphosphate diphosphohydrolase-2 (NTPDase2) inhibitors: Nucleotide mimetics derived from uridine-5′-carboxamide. *J. Med. Chem.* **2008**, *51*, 4518−4528.
(19) Seela, F.; Münster, I.; Lüchner, U.; Rosemeyer, H. 8-Azaadenosine and its 2′-deoxyribonucleoside: Synthesis and oligonucleotide base-pair stability. *Helv. Chim. Acta* **1998**, *81*, 1139−1155.
(20) Halbfinger, E.; Major, D. T.; Ritzmann, M.; Ubl, J.; Reiser, G.; Boyer, J. L.; Harden, K. T.; Fischer, B. Molecular recognition of modified adenine nucleotides by the P2Y1-receptor. 1. A synthetic, biochemical, and NMR approach. *J. Med. Chem.* **1999**, *42*, 5325−5337.
(21) Endo, T.; Zemlicka, J. Oxidation of N^6,N^6-dialkyl-2′,3′,5′-tri-*O*-acyladenosines with ruthenium tetroxide and a novel selective N-monodealkylation sequence. *J. Org. Chem.* **1979**, *44*, 3652−3656.
(22) Gillerman, I.; Fischer, B. An improved one-pot synthesis of nucleoside 5′-triphosphate analogues. *Nucleosides, Nucleotides Nucleic Acids* **2010**, *29*, 245−256.
(23) Freist, W.; Cramer, F. *Synthesis of AMP and ATP analogs*; Wiley: New York, 1978; Vol. 2, pp 827−836.
(24) Kaczmarek, E.; Koziak, K.; Sévigny, J.; Siegel, J. B.; Anrather, J.; Beaudoin, A. R.; Bach, F. H.; Robson, S. C. Identification and characterization of CD39/vascular ATP diphosphohydrolase. *J. Biol. Chem.* **1996**, *271*, 33116−33122.
(25) Smith, T. M.; Kirley, T. L. Cloning, sequencing, and expression of a human brain ecto-apyrase related to both the ecto-ATPases and CD39 ecto-apyrases. *Biochim. Biophys. Acta, Protein Struct. Mol. Enzymol.* **1998**, *1386*, 65−78.
(26) Bigonnesse, F.; Lévesque, S. A.; Kukulski, F.; Lecka, J.; Robson, S. C.; Fernandes, M. J. G.; Sévigny, J. Cloning and characterization of mouse nucleoside triphosphate diphosphohydrolase-8. *Biochemistry* **2004**, *43*, 5511−5519.
(27) Lecka, J.; Rana, M. S.; Sévigny, J. Inhibition of vascular ectonucleotidase activities by the pro-drugs ticlopidine and clopidogrel favours platelet aggregation. *Br. J. Pharmacol.* **2010**, *161*, 1150−1160.
(28) Belli, S. I.; Goding, J. W. Biochemical characterization of human PC-1, an enzyme possessing alkaline phosphodiesterase I and nucleotide pyrophosphatase activities. *Eur. J. Biochem.* **1994**, *226*, 433−443.
(29) Jin-Hua, P.; Goding, J. W.; Nakamura, H.; Sano, K. Molecular cloning and chromosomal localization of PD-Iβ(PDNP3), a new member of the human phosphodiesterase I genes. *Genomics* **1997**, *45*, 412−415.
(30) Bradford, M. M. A rapid and sensitive method for the quantitation of microgram quantities of protein utilizing the principle of protein-dye binding. *Anal. Biochem.* **1976**, *72*, 248−254.
(31) Baykov, A. A.; Evtushenko, O. A.; Avaeva, S. M. A malachite green procedure for orthophosphate determination and its use in alkaline phosphatase-based enzyme immunoassay. *Anal. Biochem.* **1988**, *171*, 266−270.
(32) Dixon, M. Graphical determination of equilibrium constants. *Biochem. J.* **1965**, *94*, 760−762.
(33) Vollmayer, P.; Clair, T.; Goding, J. W.; Sano, K.; Servos, J.; Zimmermann, H. Hydrolysis of diadenosine polyphosphates by nucleotide pyrophosphatases/phosphodiesterases. *Eur. J. Biochem.* **2003**, *270*, 2971−2978.
(34) Zebisch, M.; Sträter, N. Structural insight into signal conversion and inactivation by NTPDase2 in purinergic signaling. *Proc. Natl. Acad. Sci. U.S.A.* **2008**, *105*, 6882−6887.
(35) Gasteiger, E.; Gattiker, A.; Hoogland, C.; Ivanyi, I.; Appel, R. D.; Bairoch, A. ExPASy: the proteomics server for in-depth protein knowledge and analysis. *Nucleic Acids Res.* **2003**, *31*, 3784−3788.
(36) Larkin, M. A.; Blackshields, G.; Brown, N. P.; Chenna, R.; McGettigan, P. A.; McWilliam, H.; Valentin, F.; Wallace, I. M.; Wilm, A.; Lopez, R.; Thompson, J. D.; Gibson, T. J.; Higgins, D. G. Clustal W and Clustal X version 2.0. *Bioinformatics* **2007**, *23*, 2947−2948.
(37) Accelrys. *Discovery studio modeling environment, 2.5*; 2009.
(38) Sippl, M. J. Recognition of errors in three-dimensional structures of proteins. *Proteins* **1993**, *17*, 355−362.
(39) Wiederstein, M.; Sippl, M. J. ProSA-web: Interactive web service for the recognition of errors in three-dimensional structures of proteins. *Nucleic Acids Res.* **2007**, *35*, W407−W410.
(40) Banks, J. L.; Murphy, R. B.; Halgren, T. A.; Klicic, J. J.; Mainz, D. T.; Repasky, M. P.; Knoll, E. H.; Shelley, M.; Perry, J. K.; Shaw, D. E.; Francis, P.; Shenkin, P. S. Glide: A new approach for rapid, accurate docking and scoring. 1. Method and assessment of docking accuracy. *J. Med. Chem.* **2004**, *47*, 1739−1749.
(41) *Glide, 5.5*; Schrödinger, Inc., New York, 2009.
(42) Friesner, R. A.; Murphy, R. B.; Repasky, M. P.; Frye, L. L.; Greenwood, J. R.; Halgren, T. A.; Sanschagrin, P. C.; Mainz, D. T. Extra precision glide: docking and scoring incorporating a model of hydrophobic enclosure for protein−ligand complexes. *J. Med. Chem.* **2006**, *49*, 6177−6196.
(43) Donohue, J.; T, K. N. Base pairing in deoxyribonucleic acid. *J. Mol. Biol.* **1960**, *2*, 363−371.
(44) Åqvist, J.; Medina, C.; Samuelsson, J.-E. A new method for predicting binding affinity in computer-aided drug design. *Protein Eng.* **1994**, *7*, 385−391.
(45) Hansson, T.; Marelius, J.; Aqvist, J. Ligand binding affinity prediction by linear interaction energy methods. *J. Comput.-Aided Mol. Des.* **1998**, *12*, 27−35.
(46) Marelius, J.; Kolmodin, K.; Feierberg, I.; Aqvist, J. Q: a molecular dynamics program for free energy calculations and empirical valence bond simulations in biomolecular systems. *J. Mol. Graph Model.* **1998**, *16*, 213−225.
(47) Jorgensen, W. L.; Maxwell, D. S.; Tirado-Rives, J. Development and resting of the OPLS all-atom force field on conformational energetics and properties of organic liquids. *J. Am. Chem. Soc.* **1996**, *118*, 11225−11236.
(48) King, G.; Warshel, A. A surface constrained all-atom solvent model for effective simulations of polar solutions. *J. Chem. Phys.* **1989**, *91*, 3647−3661.

(49) Gillerman, I.; Fischer, B. Investigations into the origin of the molecular recognition of several adenosine deaminase inhibitors. *J. Med. Chem.* **2011**, *54*, 107−121.
(50) Gillerman, I.; Fischer, B. An improved one-pot synthesis of nucleoside 5′-triphosphate analogues. *Nucleosides, Nucleotides Nucleic Acids* **2010**, *29*, 245−256.
(51) Ludwig, J. A simple one flask synthesis of nucleoside 5′-triphosphates from unprotected nucleosides via nucleoside 5′-cyclotriphosphates. In *Biophosphates and Their Analogues—Synthesis, Structure, Metabolism and Activity*; Proceedings of the Second International Symposium on Phosphorus Chemistry Directed Towards Biology, Lodz, Poland, Sep 8−12, 1986; Elsevier Science Publishers B. V.: Amsterdam, Netherlands,1987; p 201.
(52) Kukulski, F.; Sévigny, J.; Komoszynski, M. Comparative hydrolysis of extracellular adenine nucleotides and adenosine in synaptic membranes from porcine brain cortex, hippocampus, cerebellum and medulla oblongata. *Brain Res.* **2004**, *1030*, 49−56.
(53) Zebisch, M.; Krauss, M.; Schaefer, P.; Straeter, N. Crystallographic evidence for a domain motion in rat nucleoside triphosphate diphosphohydrolase (NTPDase) 1. *J. Mol. Biol.* **2012**, *415*, 288−306.
(54) Zebisch, M.; Krauss, M.; Schaefer, P.; Lauble, P.; Straeter, N. Crystallographic snapshots along the reaction pathway of nucleoside triphosphate diphosphohydrolases. *Structure (Oxford, U. K.)* **2013**, *21*, 1460−1475.
(55) Sévigny, J.; Sundberg, C.; Braun, N.; Guckelberger, O.; Csizmadia, E.; Qawi, I.; Imai, M.; Zimmermann, H.; Robson, S. C. Differential catalytic properties and vascular topography of murine nucleoside triphosphate diphosphohydrolase 1 (NTPDase1) and NTPDase2 have implications for thromboregulation. *Blood* **2002**, *99*, 2801−2809.
(56) Wink, M. R.; Braganhol, E.; Tamajusuku, A. S. K.; Lenz, G.; Zerbini, L. F.; Libermann, T. A.; Sévigny, J.; Battastini, A. M. O.; Robson, S. C. Nucleoside triphosphate diphosphohydrolase-2 (NTPDase2/ CD39L1) is the dominant ectonucleotidase expressed by rat astrocytes. *Neuroscience* **2006**, *138*, 421−432.
(57) Langer, D.; Ikehara, Y.; Takebayashi, H.; Hawkes, R.; Zimmermann, H. The ectonucleotidases alkaline phosphatase and nucleoside triphosphate diphosphohydrolase 2 are associated with subsets of progenitor cell populations in the mouse embryonic, postnatal and adult neurogenic zones. *Neuroscience* **2007**, *150*, 863−879.
(58) Knowles, A. F.; Chiang, W.-C. Enzymatic and transcriptional regulation of human ecto-ATPase/E-NTPDase 2. *Arch. Biochem. Biophys.* **2003**, *418*, 217−227.
(59) Buffon, A.; Ribeiro, V. B.; Wink, M. R.; Casali, E. A.; Sarkis, J. J. Nucleotide metabolizing ecto-enzymes in Walker 256 tumor cells: molecular identification, kinetic characterization and biochemical properties. *Life Sci.* **2007**, *80*, 950−958.
(60) Cornish-Bowden, A. A simple graphical method for determining the inhibition constants of mixed, uncompetitive and non-competitive inhibitors. *Biochem. J.* **1974**, *137*, 143−144.
(61) Lecka, J.; Bloch-Boguslawska, E.; Molski, S.; Komoszynski, M. Extracellular purine metabolism in blood vessels (Part II): Activity of ecto-enzymes in blood vessels of patients with abdominal aortic aneurysm. *Clin. Appl. Thromb./Hemostasis* **2010**, *16*, 650−657.
(62) Boukharta, L.; Keranen, H.; Stary-Weinzinger, A.; Wallin, G.; de Groot, B. L.; Aaqvist, J. Computer simulations of structure−activity relationships for hERG channel blockers. *Biochemistry* **2011**, *50*, 6146−6156.